129456

ANALYSIS OF CIRCULAR WAVEGUIDE MODES

by

LEOPOLD B. FELSEN

Final Report R-484-56, PIB-414

for

SIGNAL CORPS ENGINEERING LABORATORIES
Contract DA-36-039 sc-64424
Dept. of the Army Project No. 3-99-15-022
Signal Corps Project No. 152B
May 3, 1956

MRI

POLYTECHNIC INSTITUTE OF BROOKLYN
MICROWAVE RESEARCH INSTITUTE

Microwave Research Institute
Polytechnic Institute of Brooklyn
55 Johnson Street
Brooklyn 1, New York

Report R-484-56, PIB-414
Dept. of the Army Project No.
3-99-15-022
Signal Corps Project No. 152B

FINAL REPORT

ANALYSIS OF CIRCULAR WAVEGUIDE MODES

Prepared for
Department of the Army
Signal Corps Engineering Laboratories
Under
Contract DA-36-039 sc-64424
Squier Signal Laboratory Technical Requirements, dated 12 February 1954,
For PR & C No. 54/ELS/R-3318

Title Page
Abstract
Table of Contents (2 Pages)
19 Pages of Text
Appendix I
16 Pages of Figures

Author: L. B. Felsen
L. B. Felsen
Research Assistant Professor

Approved:
Ernst Weber
Director

Brooklyn 1, New York
May 3, 1956

ABSTRACT

The research on this contract has been concerned with a theoretical and experimental investigation of propagation of electromagnetic waves in uniform waveguide regions capable of supporting several propagating modes, with special application to circular waveguide. The theoretical aspect comprises three main phases: a) investigation of mode characteristics in circular waveguide, b) description of lumped discontinuities in multimode waveguide, and c) propagation through two or more isolated discontinuities in multimode waveguide. Included in the first category are the determination of attenuation constant, cutoff wavelength, and power capacity of any particular circular waveguide mode, as well as a study of power coupling between orthogonal modes in circular guide with lossy walls. Comprehensive plots and tabulations have been made for all modes which can propagate up to the TE_{02}.

The lumped discontinuities investigated include arbitrary small transverse or longitudinal apertures and obstacles, angularly symmetric discontinuities (centered circular apertures and disks of varying sizes), and pseudo-symmetric discontinuities (symmetrical arrangements of symmetrical obstacles or apertures in the guide cross section). The general small obstacle and aperture study has yielded first-order theoretical results which are applicable in arbitrary multimode guide in the limit of small discontinuity dimensions. A quantitative check of the small obstacle and aperture, as well as other, approximate formulas was obtained by their application to TE_{01} mode coupling via angularly symmetric and pseudo-symmetric discontinuities in circular waveguide, and subsequent comparison with experimental results. Comprehensive data and comparison with theory for the above-mentioned structures have been presented. Calculations have also been carried out for the effect of asymmetries on coupling into undesired modes.

The network problem of propagation in multimode waveguide through two or more isolated discontinuities has been analyzed in terms of a transfer operator which relates directly the network quantities at one terminal plane to those at another, thus facilitating the study of cascaded structures. Various alternative representations for the transfer operator (in either an impedance or scattering basis) have been obtained, their relationships pointed out, and restrictions imposed by reciprocity, conservation of energy, and symmetry have been formulated. A Table has been presented for the various transfer representations for particular simple structures. The formalism has been applied to the study of multimode propagation through two transverse discontinuities.

A cavity setup for the experimental measurement of TE_{01} mode discontinuities in circular waveguide has been constructed and permits measurements with a high degree of precision.

TABLE OF CONTENTS

TABLE OF CONTENTS (Cont.)

I. Purpose

The purpose of this contract is the theoretical and experimental investigation of the behavior of mode fields in multimode circular waveguide, and of the interaction between modes in discontinuity regions.

II. Conferences

Mr. Donald Rouse of the Signal Corps met with Drs. L. Felsen, N. Marcuvitz, and Mr. W. Kahn on October 5, 1955 and January 24, 1956. Future program and the Final Report, respectively, were discussed at these meetings.

III. Factual Data

A. Introduction

The research conducted on this contract has been concerned with a theoretical and experimental investigation of propagation of electromagnetic waves in uniform waveguide regions capable of supporting several propagating modes, with special application to circular waveguide. The theoretical study comprises three main phases: 1) investigation of mode characteristics in circular waveguide; 2) description of lumped discontinuities in multimode waveguide; and 3) propagation through two or more isolated discontinuities in multimode waveguide. The first category is clearly specialized to circular waveguide although some results are also characteristic of other multimode systems; the results obtained in the second and third categories are valid for arbitrary uniform waveguide regions, but examples for computation have been selected from circular waveguide configurations.

At millimeter wavelength applications, toward which the studies on this contract are ultimately directed, the use of oversized (multimode) waveguide becomes desirable in view of the required small size of appropriate single-mode guides. Circular waveguide is convenient in this connection because of its comparative ease of manufacture. Moreover, the circular electric (TE_{0n}) modes in circular waveguide are of particular interest for low-loss transmission in view of their anomalous attenuation property which yields a decreasing attenuation constant with increasing frequency. Their high degree of symmetry makes it relatively simple to obtain a TE_{0n} mode system by the use of radial fin mode filters (Fig. 1(c)) which pass TE_{0n}, but attenuate all other modes. For the design of components it appears desirable, at least initially, to restrict TE_{0n} mode propagation to the TE_{01} mode (i.e., TE_{0n} modes are beyond cutoff, $n \geq 2$). The problems of coupling into other modes, which are present even under these conditions since TE_{01} is not the lowest circular waveguide mode, are thereby minimized. The transition from a TE_{0n} mode system ($n > 1$) desirable for long-range transmission to a TE_{01} system can be effected by slowly tapering from the TE_{0n} guide radius to one small enough to propagate only the TE_{01} mode. Subsequent

advances in technique may make it possible, or even beneficial, to exploit the presence of more than one desired propagating mode in component design.

The experimental phase of this contract has been concerned with the measurement of TE_{01} mode discontinuities in circular waveguide. Although the measurement is one in a single mode, the measurement technique must be such as to discriminate against other undesired modes which are likewise present. The purpose of the measurements has been mainly to check the accuracy of theoretical formulas derived for a variety of configurations.

The results obtained in both the theoretical and experimental phases are summarized below. If detailed considerations have been given in the various Quarterly Reports[1], they are not repeated here. Instead, reference is made to the appropriate material which has been reported previously.

B. Mode Characteristics in Circular Waveguide

The study of mode characteristics in circular waveguide began with such problems as the determination of (wall-loss) attenuation constant, cutoff wavelength, power capacity, etc., for any circular waveguide mode. Some of this materials is, of course, available in the literature, and effort in those instances has been expended primarily in compiling more comprehensive tabulations of the desired quantities.

1. Attenuation

Calculations of the wall-loss attenuation constant α have been made for all modes which can propagate in a circular guide up to, and including, the TE_{02} mode. The results of α vs. a/λ are presented in graphical form in Q1, Figs. MRI-14588 to MRI-14591, where a is the guide radius and λ is the free-space wavelength.

2. Cutoff Wavelength

A chart has been plotted for the cutoff wavelength λ_c vs. a for all modes for which $(a/\lambda_c) < 2$ (Q1, Figs. MRI-14592 and MRI-14593).

3. Power Capacity (Q2, Sec. III A)

To determine the power capacity in any given circular waveguide mode, an investigation was made of the maximum electric field for each mode. It was shown first that, for any propagating TM mode in a uniform waveguide, the maximum electric field vector is either longitudinal or transverse. Moreover, the location in the guide cross section of the maximum electric field vector is independent of frequency for TE modes, while for TM modes, the locations of the maximum transverse and longitudinal electric field components, respectively, are independent of frequency. For circular waveguide, it was shown in addition that the maximum electric field for TE_{mn} modes is azimuthal, $m = 0$, and radial when $m \neq 0$, while for TM modes, the maximum electric field is azimuthal when it is transverse.

---

[1] Quarterly Reports 1 through 5 will be abbreviated by Q1, ... Q5.

Calculations have been carried out and plotted vs (a/λ) for the power capacity and the maximum electric field location for all TE and TM modes which can propagate up to TE_{02}. For TM modes the relative wavelength for which the maximum electric field direction changes from transverse to longitudinal have also been computed. The graphs permit a determination of the power capacity in a given mode corresponding to a specified allowable value of maximum electric field based on dielectric breakdown considerations.

4. Attenuation of Finned and Sectoral TE_{01} Waveguide

Since propagation in the TE_{01} mode in circular waveguide (Fig. 1(a)) is often conveniently analyzed in terms of propagation in an equivalent sectoral guide (Fig. 1(b)), the modes in the latter have likewise received attention (Q3, Sec. III B2). Moreover, the TE_{01} attenuation in a finned circular guide

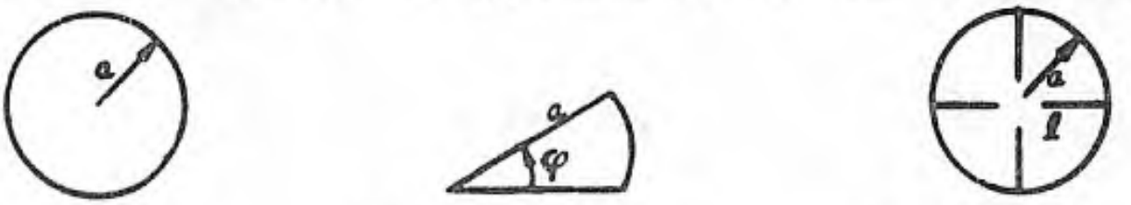

(a) CIRCULAR (ℓ) SECTORAL (c) FINNED

Fig. 1 - Waveguide Configurations.

(Fig. 1(c)), which arises in connection with a metallic radial fin mode filter, has been computed and plotted as a function of ℓ/a, where ℓ is the radial extent of the fin, for values $0 < \ell/a \leq 1$ (Q3, Sec. III C, and Figs. MRI-1500$\frac{4}{5}$ and MRI-1500$\frac{5}{4}$). For $\ell = a$, the finned waveguide problem becomes identical with that in sectoral guide.

5. "Power Coupling" Between Orthogonal TE_{0m} Modes in Lossy Circular Guide

The computation of the power loss due to dissipation in the guide walls from the modal attenuation constant is well known for the case where any given mode propagates by itself in the waveguide. However, when a number of modes propagate simultaneously down the guide, the power loss in a length L of waveguide is generally not given by the sum of the power losses obtained when each mode propagates separately, although the modes are orthogonal over the guide cross section. This problem of "power coupling" between orthogonal modes has been investigated in detail for a circular waveguide propagating several TE_{0m} modes simultaneously (Q3, Sec. III A). It was found that for loss computations over short lengths L of waveguide, the power coupling is significant and yields a power loss which, for any given pair of modes, varies sinusoidally with L. For long lengths L, on the other hand, the coupling is insignificant and the power loss may be computed as though each mode were propagating separately.

C. Discontinuities in Multimode Waveguide

1. Formal Theory

The propagation properties of electromagnetic fields in an empty waveguide supporting N orthogonal, propagating modes can be rigorously described in terms of the behavior of the voltages and currents on N uncoupled transmission lines. If a lumped discontinuity is introduced into the waveguide (Fig. 2(a)) an infinity of waveguide modes is required to satisfy the electromagnetic boundary conditions in the discontinuity region; however, "far" from the discontinuity the field behavior can be described solely in terms of the N propagating modes. The effect of the discontinuity on the far fields is to relate the previously independent far field mode amplitudes. In terms of the network equivalent, this mode interaction at the discontinuity is represented by means of a network coupling the N transmission lines (Fig. 2(b)), where the

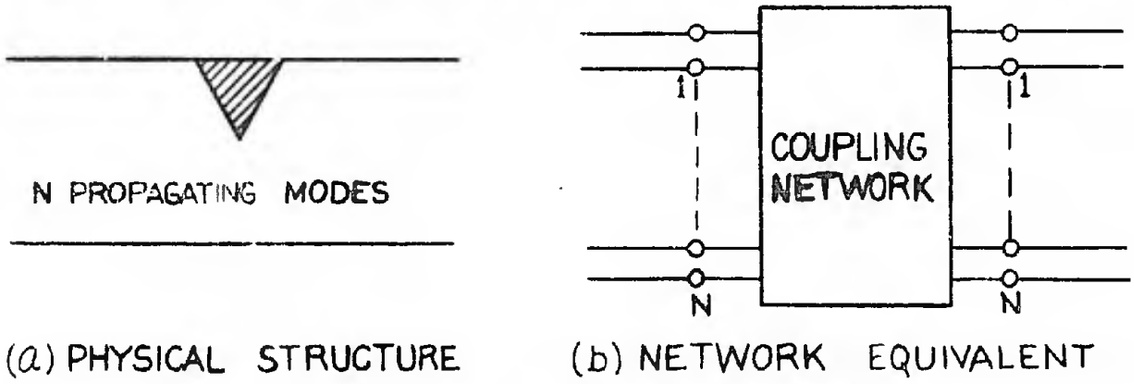

Fig. 2 - Discontinuity in Multimode Waveguide.

network terminals are assumed to be located "far" from the discontinuity region. ("Far" in this context implies that the amplitude of any non-propagating mode generated at the discontinuity is negligible at the network terminals). If the parameters of the coupling network are known, the voltage-current behavior along the various transmission lines, and thereby the electromagnetic field behavior outside the discontinuity region, is completely determined.

A general formalism via an integral equation method has been developed for the determination of the coupling network parameters for transverse (Fig. 3(a)) and longitudinal (Fig. 3(b)) aperture discontinuities (see Q1, Appendix I), and

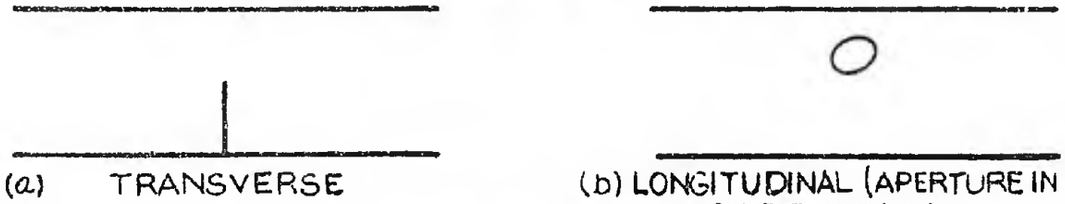

Fig. 3 - Special Discontinuities.

for transverse obstacle discontinuities (Fig. 3(a)) (see Q3, Sec. III B1). (An alternative and more direct description from a "scattering" viewpoint has been under consideration and will be discussed under the successor contract.) Although the network parameters are defined by variational expressions, their evaluation therefrom for any particular configuration is nevertheless cumbersome and difficult. Stress has therefore been placed on simple approximate methods of evaluation which fall into two categories: 1) small aperture and small obstacle techniques, valid when the aperture or obstacle dimensions are small compared to the wavelength, and 2) "equivalent stored power" techniques, whereby one attempts to relate a given unknown discontinuity problem to a known problem involving a similar field configuration in a different geometry.

2. Small Aperture and Obstacle Techniques

A technique for obtaining approximate solutions for small aperture discontinuities in waveguides in terms of known "static" approximate solutions in free space is due to Bethe. Via this technique, the far field effect of the (small) aperture or obstacle is obtained from equivalent electric and magnetic dipoles in the discontinuity-free waveguide. The strengths of these dipoles are specified in terms of the polarizabilities of the aperture (or obstacle) which are known either theoretically or experimentally for a variety of configurations. By applying an equivalent network viewpoint (see Section I) to this problem, whereby the dipoles are represented as voltage and current generators on a transmission line, the computation of the fields scattered by the discontinuity (i.e., the determination of the scattering matrix for the structure) becomes simple and direct (Q1, Appendix I, Secs. 1b and 2b, and Q3, Sec. III B1b). Explicit results for the scattering matrix have been obtained for transverse obstacles (Q3, Eqs. (26) and (31)) and for the following aperture coupling configurations: a) transverse-transverse (Fig. 4(a)) (Q1, Eqs. (6), (9), (11); in Eq. (6), $j\omega\epsilon$ should be replaced by $j/\omega\epsilon$); b) transverse-longitudinal (Fig. 4(b)) (Q2, Eqs. (78)-(79); c) longitudinal-longitudinal (Fig. 4(c)) (Q2, Eqs. (70)-(71)). The formulas presented permit the direct computation of the power scattered by the discontinuity into any one mode due to a specified incident mode.

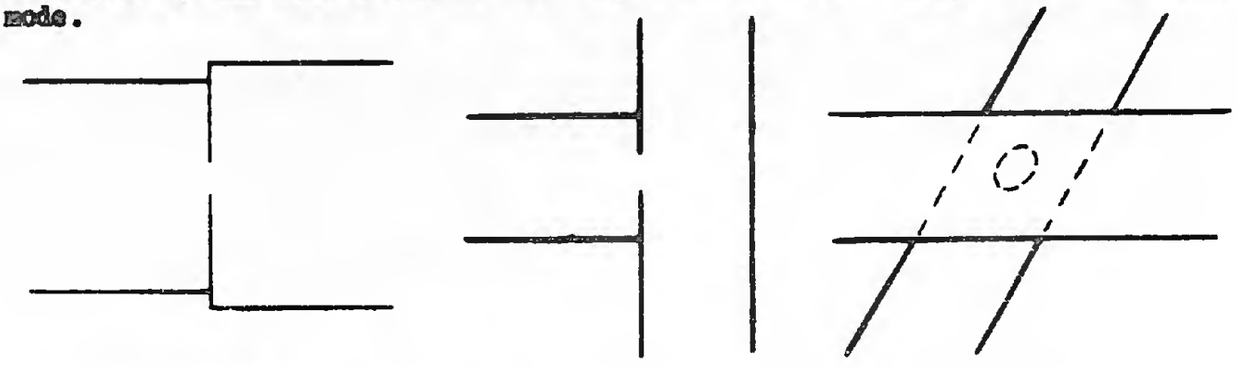

(a) TRANSVERSE-TRANSVERSE (b) TRANSVERSE – LONGITUDINAL (c) LONGITUDINAL – LONGITUDINAL

Fig. 4 - Types of Aperture Coupling

The effect of wall thickness in aperture coupling was likewise investigated (Q2, Sec. III B3).

The above mentioned approximate formulas for the scattering matrix for various aperture and obstacle configurations are expected to be valid if a) the discontinuity dimensions are "small" compared to the wavelength, b) transverse discontinuities are located "not near" the guide walls, and c) the radius of curvature of the guide wall containing a longitudinal aperture is "large" compared with the aperture dimensions. Quantitative estimates of what is meant by the terms"small", "not near", and "large" as employed above require either a detailed theoretical analysis (which is usually extremely difficult) or experimental investigation. The latter course has been adopted on this contract, and experimental measurements have been taken over a range of frequencies on the various transverse obstacle and aperture configurations given below. So far, the measurements have been of the one-mode type (TE_{01} mode in circular waveguide), but multimode measurements are planned under the successor contract. Experimental results and comparisons with theory are given in Sec. 3. In view of the agreement obtained it is felt that even for the multimode case under comparable conditions of "smallness", etc., the above-mentioned approximate expressions will yield correct order-of-magnitude results.

3. Theoretical and Experimental Results for Various Transverse Circular Waveguide Discontinuities

a) Centered Circular Aperture (TE_{01} mode) ($.896a < \lambda < 1.640a$)

The TE_{01} mode equivalent circuit is a shunt inductance (TE_{0n} modes, $n \geq 2$, are beyond cutoff). For small aperture radius "b", the first-order small aperture theory discussed above yields infinite susceptance, i.e., the

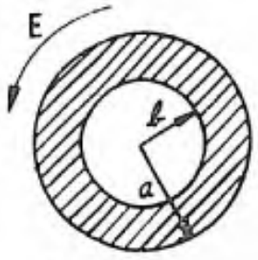

Fig. 5 - Centered Circular Aperture.

discontinuity is of a higher order of magnitude; its determination will be considered in the future. For larger apertures ($.5a < b < a$), a variational calculation for the susceptance and experimental verification was carried out by Sheingold[2]. Since his theoretical results are in the form of an infinite series which makes computation cumbersome, a simple approximate expression has been

---

[2] L. S. Sheingold, "The Susceptance of a Circular Obstacle to an Incident Dominant Circular-Electric Wave", Cruft Lab., Harvard U., Technical Report No. 159, June 15, 1952.

derived from "equivalent stored power" considerations (Q2, Eq. (66)), and has subsequently been slightly modified into the form given in Fig. MRI-15572. It is seen that reasonable agreement is found with the experimental measurements for $(b/a) \geq .8$, for the three frequencies tested: $a/\lambda = .65, .75, .90$. The complete experimental data for the same three a/λ ratios starting from $b/a = .5$ in steps of .05 has been plotted in Fig. MRI-15574. The measurements for $a/\lambda = .90, .65$ were carried out by a semi-precision (multipoint) method, while those at $a/\lambda = .75$ were obtained from single-point measurements. General agreement with Sheingold's data was obtained.

b) Centered Circular Disk (TE_{01} Mode)

The TE_{01} mode equivalent circuit is a shunt inductance. For $r_o/a \ll 1$,

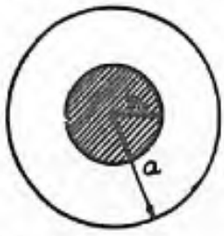

Fig. 6 - Centered Circular Disk.

a small obstacle result was derived (Q3, Eq. (38)); for $r_o/a \approx 1$, another approximate expression was obtained from "stored power" considerations (Q3, Eq. (42)). A variational calculation carried out by Barnard (cf. Q4, p. 1-4) yielding upper and lower bounds on the susceptance indicated that the small obstacle formula is very good for $r_o/a \leq .2$, and reasonably good even up to $r_o/a \approx .45$ (Q4, Fig. MRI-15176). Experimental measurements verified these observations for the small disk range $r_o/a \leq .2$ (see Fig. MRI-15575). Over the extended range of $r_o/a > .2$, the small obstacle formula yields good results for $a/\lambda = .65$ even up to $r_o/a \approx .50$, but poorer results (magnitude of B too large) for $a/\lambda = .75$, and especially for $a/\lambda = .90$ (see Fig. MRI-15576). The complete set of experimental measurements on disks varying from $.5 \geq (r_o/a) \geq 0$ in steps of .05 for $a/\lambda = .65, .75, .90$ is given in Fig. MRI-15576.

In view of the favorable agreement with experiment obtained for the large aperture formula in Sec. a), it is expected that the large disk formula (Q3, Eq. (42)) is reasonably good over the range $.7 < r_o/a < 1$, with better agreement for the larger r_o/a values.

c) Off-Center Circular Disk

The configuration of a disk with radius r_o, whose center is located at

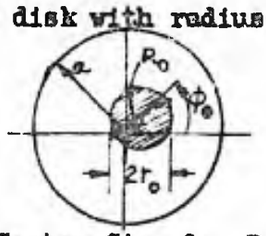

Fig. 7 - Off-Center Circular Disk.

the cylindrical coordinates R_o, Φ_o with respect to a set of reference axes, is shown in Fig. 7. Since this configuration does not possess the angular symmetry of a centered obstacle, an incident TE_{01} mode will couple to a variety of other modes. Numerical calculations of the coupling coefficients between any two modes below the TE_{02} have been made to $O(\alpha)$, where the normalized off-center shift $\alpha = R_o/a$ is assumed to be small (Q3, Figs. MRI-15000 to MRI-15002, and Q4, Table A). The results permit the direct computation of the power scattered into the various modes due to an error in centering the disk. For example, for $R_o/a \leq .07$, the (current) scattering coefficient between the TE_{01} mode and the TM_{11}, TE_{11}, and TE_{21} modes is less than 6% of the TE_{01} mode scattering coefficient of the centered obstacle, over a range of $.65 < (a/\lambda) < 1.0$, with the larger values occurring for the larger (a/λ).

d) N Symmetrically Arranged Circular Disks (TE_{01} Mode)

By arranging a number of symmetrical obstacles (or apertures) symmetrically in the guide cross section one may again achieve coupling to the TE_{01} mode only, although the complete symmetry characteristic of centered apertures or disks has been disturbed. From symmetry considerations, it is evident that the insertion of electric walls along the dotted lines in Fig. 8 will not disturb the field configuration for TE_{01} mode incidence. Thus, the basic propagation

Fig. 8 - Four Symmetrically Arranged Circular Disks.

problem is identical with that in a sectoral guide with angle $\gamma = \pi/N$ (Fig. 1(b)), where N is the number of obstacles (apertures). It is readily ascertained (Q3, Sec. III B2) that an incident TE_{01} mode excites no other propagating modes for: $N = 3$, $\lambda > 1.50a$; $N = 4$, $\lambda > 1.18a$; $N = 5$, $\lambda > .98a$; $N = 6$, $\lambda > .84a$. (Note: TE_{01} cutoff is at $\lambda = 1.640a$). Since the TE_{02} mode propagates for $\lambda < .90a$, one must maintain $\lambda > .90a$ so that no gain in frequency range is achieved by the use of more than six obstacles (apertures).

The TE_{01} mode equivalent circuit for a symmetrical arrangement of N small circular disks is a shunt susceptance which is capacitive for disk locations in the vicinity $R \approx a/2$. (Note: For $R = 0$ (centered disk) and for $R = a$ (semi-disks on guide wall) the susceptance is inductive.) The formula derived for the susceptance from small obstacle considerations is given in Q3, Eq. (44), where it is assumed that each disk contributes to the susceptance as though the other disks were absent. A further theoretical investigation showed that interaction between disks is negligible if it can be assumed that a) r_o/a is small, and b) that the variation over any disk area of the fields due to the currents

induced on the other disks can be neglected (this implies a certain minimum spacing between the disks). The effect of interaction was also checked experimentally by measuring the susceptance of three, four, and six disks, respectively. The susceptance per disk (at $R/a = .5$) was found to be independent of the number of disks for $r_o/a \leq .15$, $a/\lambda = .65$, and $r_o/a \leq .125$, $a/\lambda = .75$, thus verifying the theoretical conclusions (see Figs. MRI-15577 and MRI-15578).

Experimental measurements for three, four, and six disks at $a/\lambda = .65$, .75, .90 were carried out for values of $R/a = .35$, .50, .65, and of r_o/a varying from .05 to .20 in steps of .025. The results are shown in Figs. MRI-15577 - MRI-15579, and Fig. MRI-15580. The above-mentioned approximate small obstacle formula is found to yield capacitive values smaller than those measured, even for very small disks. The reason for this discrepancy is not clear at the moment and will be further investigated. If the theoretical values are made to agree with the experimental ones at the central point $R/a = .50$ by the inclusion of an empirical factor in the formula, it is found that the formula will predict quite well the susceptance values for different R/a. The appropriate empirical factor was found to be $(.82 + .6\ (a/\lambda))$ for the range $.65 < a/\lambda < .90$. Curves computed from the resulting formula listed on Fig. MRI-15577 are seen to predict the susceptance reasonably well over the above range of variables.

e) N Symmetrically Arranged Circular Apertures (TE_{01} Mode)

The equivalent circuit for N circular apertures is a shunt inductance whose value has been computed from small aperture considerations (Q3, Eq. (45)) and plotted for various values of R/a and r_o/a (Q3, Fig. MRI-14998; note: due to an error in calculation, the reactances plotted in this Figure are too large by a factor of 10).

f) Asymmetry Effect in a Symmetrical Arrangement of Circular Apertures

If one of the discontinuities in a symmetrical arrangement violates the symmetry requirement, coupling into other modes occurs. The TE_{01} mode coupling to both TE and TM modes has been computed for the case of an asymmetrically located aperture (Q3, Sec. III B3e), where r_1 and Φ_1 are the radial and angular deviations, respectively, from the symmetrical position (Fig. 9). Numerical calculations

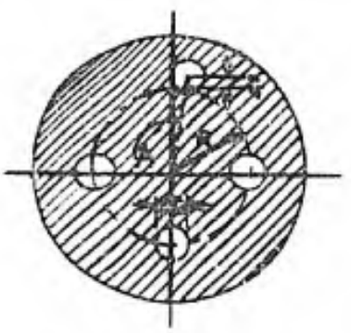

Fig. 9 - Asymmetrically Located Aperture in a Symmetrical Arrangement.

carried out for an angular deviation error only (i.e., $r_1 = 0$) show that the magnitude of the scattering coefficient between the TE_{c1} mode and the TE_{11}, TE_{21} and TM_{11} modes, respectively, is less than 1.5 x (angular error in radians) x (TE_{01} mode scattering coefficient for a symmetrical arrangement), for $.3 < (R/a) < .7$ (Q3, Fig. MRI-15003).

g) Transverse Discontinuity Coupling Two Different Dielectric Media

In order to support physically such discontinuity structures as centered disks, etc., it is often necessary to mount the structures on the face of a slab of dielectric completely filling the waveguide (Fig. 10). This necessitates an investigation of how the value of a discontinuity computed on the basis

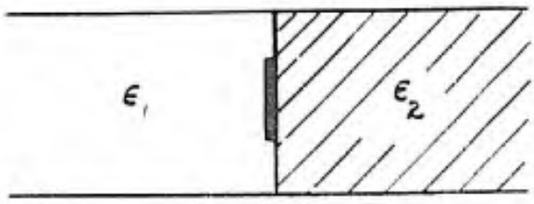

Fig. 10 - Transverse Discontinuity at Dielectric Interface.

of a continuous medium is affected by the presence of the dielectric. A detailed theoretical formulation in multimode guide of this effect for both apertures and obstacles has been carried out (Q4, Sec. III A5). Numerical calculations from a variational expression have been made for special cases of a centered circular disk and aperture with TE_{01} mode incidence (single-mode problem), with the assumption that $\epsilon_2 \simeq \epsilon_1$. For the circular disk it was found that the correction to the shunt reactance X_0 appropriate to $\epsilon_1 = \epsilon_2$ is less than $\alpha\left[(\epsilon_2/\epsilon_1) - 1\right] X_0$ for $r_0/a \leq .5$, where $\alpha = 1/7$, $a/\lambda = .75$, and $\alpha = 1/3$, $a/\lambda = .90$. Thus, the correction is certainly negligible for such materials as polyfoam, as was verified experimentally. It is of interest to note, however, that the frequency dependence of the correction term is found to be stronger than that of X_0 (see Q4, p. 24) (see also Fig. MRI-15581).

D. Network Calculations in Multimode Waveguide

The investigation of propagation through several lumped discontinuities in a waveguide poses a simple network problem for single-mode guides, but becomes formidable in detail when several propagating modes are involved. The transformation of pertinent network quantities (such as voltage-current, or incident-reflected waves) from one terminal plane to another past several intervening structures is carried out most directly in terms of a transfer operator which relates quantities at the input side of a network to those at the output side, so that the overall result of an interconnection of networks is described by the product of the individual transfer operators. Two basic transfer formulations have been considered (Q5, Sec. III A): 1) in terms of voltages and currents (impedance transfer description), and 2) in terms of incident and reflected waves (scattering transfer description). Within each of these formulations,

additional representations can be found depending on the ordering of the matrix elements.

The various transfer representations alluded to above have been considered from a unified viewpoint from which any particular representation can be inferred when desired. Relationships between the various representations have been obtained, as have the conditions imposed by such network properties as reciprocity, symmetry, conservation of energy. The various transfer representations for such simple structures as a length of waveguide, a dielectric interface, and a shunt discontinuity have been listed. Moreover, the simple example of propagation past two lumped discontinuities in multimode waveguide has been considered in detail by a scattering transfer formulation, and solved explicitly for small discontinuities by an approximation procedure. The results are of interest for the compensating problem whereby a discontinuity is employed to correct some effects which are unavoidably introduced by some residual discontinuity caused by mechanical imperfections, etc., in the waveguide.

D. Experimental Phase (W. K. Kahn)

1. General Description of Equipment*

The resonance measuring setup is schematized in Fig. MRI-15582. As may be seen from this figure the system comprises three main assemblies: the microwave source assembly, the frequency monitoring assembly, and the cavity assembly. These assemblies are interconnected via coaxial transmission lines, RG-9/U being employed for the direct connections from oscillator to the measuring cavity. Only the cavity assembly will be described in some detail. The remaining assemblies are composed of standard commercial components, the functions of which will require only brief comment. The particular components themselves are listed in Appendix I. A photograph of the resonance measuring setup is shown in Fig. MRI-15384.

a) Source Assembly

The source of microwave energy is a klystron tube, the repeller of which is square wave modulated at 1000 cycles/sec. The modulation envelope is recovered at the crystal detector and displayed on the oscilloscope as an aid in tuning.[3] The attenuator serves to isolate the oscillator in the usual fashion.

---

* Acknowledgment is due to Mr. Paul Mariotti of M.R.I. staff for his aid in resolving some of the mechanical problems involved in the construction of the measuring cavity.

3 "Instruction Manual on Equivalent Circuit Measurements of Waveguide Structures", Microwave Research Institute, Polytechnic Institute of Brooklyn, Research Report R-284-52, PIB-223, March 1953, pg. 5 et seq.

The low-pass filter was inserted to preclude spurious responses of the measuring cavity to harmonics of the fundamental oscillator frequency.

b) Frequency Monitoring Assembly

The essential element of this assembly is the transmission wavemeter. It consists of cavity formed by a coaxial transmission line with fixed short circuit at one end and a movable short circuiting plunger at the other. This is an absolute instrument in that the wavelength is obtained directly from the difference between successive plunger positions in which the cavity is resonant, i.e., transmits maximum power to the amplifier.

c) Cavity Assembly

The cavity assembly is shown diagrammatically at the bottom of Figure MRI-15582. It comprises the measuring cavity plus a detector and amplifier system. When the cavity is near resonance in the desired mode, the detecting probes transmit an appreciable signal to the detector. At the detector, the 1000 ~ modulation is recovered; it is then amplified to provide the meter indication.

The measuring cavity is the essential component of the resonance measuring setup. It is a length of smooth waveguide short circuited at both ends by adjustable plungers, with provision for inserting some desired discontinuity and with coupling arrangements for injection and sampling of R.F. energy. The general requirements for such a device were discussed in the Introduction, part B, of Q4. The particular design was based on a cavity of the same type described by Sheingold.[4] The measuring cavity was constructed in halves, one of which is shown in cross section on MRI-15499. The remaining half mates with the circular waveguide flange of the first and is very similar to it. It differs only in that it carries no coupling probes, and in the increased travel of the short-circuiting plunger made possible by the absence of these probes.

The terms employed in the following description which refer to parts of the measuring cavity are defined directly on the drawing MRI-15499. The circular waveguide walls of the measuring cavity are sections of commercial brass tubing nominally 6" O.D. 1/8" wall thickness. The short-circuiting plungers, which form the end plates of the cavity, are also brass and are non-contacting. A dielectric support (polystyrene) rides on the inner walls of the circular waveguide and mates with the brass short-circuiting plate. No choke arrangement is required by the desired H_{01} mode fields. Energy which leaks past the plunger (excited, perhaps, by spurious modes) is absorbed in lossy material, Spongex,[5] placed there.

---

[4] L. S. Sheingold, "An Experimental Investigation of the Transmission Properties of the Dominant Circular-Electric Mode", Technical Report No. 167, Cruft Laboratory, Harvard University, Cambridge, Massachusetts, September 1953.

[5] Brochure: "Microwave Absorbents". The Sponge Rubber Products Company, Shelton, Connecticut.

A precision drive was constructed for the short-circuiting plungers. The mechanism is simple. As the precision drive screw is rotated via the drive wheel, the tie plate travels along the screw. The tie plate causes the three drive rods to push (or pull) symmetrically on the plunger. The precision 1/2" diameter steel screw was especially ground to an estimated accuracy of ± .0005" with 20 threads/inch. The tie plate bears along 1-1/2 inches of this screw via a bronze bearing. The drive rods are 1/2 in.dia. steel drill rods which pass through bronze bearing supports, enter the cavity, and are attached to the brass plunger face. The length of the drive rods, i.e., the plunger travel, is restricted so that the plunger cannot come into contact with any of the probes which project into the cavity from the waveguide walls.

The rim of the drive wheel is graduated in terms of hundredths of a revolution (.0005 in.). A revolution counter is coupled to the precision screw via a set of gears so that the last digit counts every tenth of a revolution (.005 in.). The counter may be reset to zero for any arbitrary reference position.

The flange which connects the two halves of the measuring cavity is of the butt type described (for rectangular waveguide) in previous MRI reports.[6] The discontinuities to be measured were inserted into the cavity at this flange. Discontinuities, consisting of apertures in thin transverse conducting sheets, were cut from brass disks with approximately the O.D. of the cavity waveguide. These disks therefore made direct contact with the waveguide which protrudes from the butt flange. They were centered by means of a simple jig fitting on the outside of the protruding waveguide. The jig is shown in Fig. MRI-15583. This jig remains in place between the butt flanges during the measurement. Discontinuities consisting of conducting obstacles not making contact with the guide walls were mounted on polyfoam pillboxes and inserted into the cavity waveguide.

The location of the probes (seven shielded magnetic loops) is shown in Fig. MRI-15499. The generator probe, mounted in the plunger face at the radial location of the maximum of the H^{o}_{01} mode magnetic field, is connected to the microwave source. The two monitoring probes are mounted 45° apart in a transverse plane. The four detector probes are mounted 90° apart in a transverse plane. They are symmetrically interconnected as shown schematically in Fig. MRI-15584 by coaxial (RG-9/U) lines and coaxial UG-21 B/U Tees. The lengths of line were made of equal physical length so that (electrical) symmetry is independent of frequency.

The construction of the shielded magnetic loop probes used as monitoring and detecting probes is shown in the drawing MRI-15500. The excitation loop is identical with these except for the external contours which have been modified to suit its particular location. One feature, the thin coaxial line, requires comment. The inner conductor and dielectric (Teflon) were taken from a commercial

---

6 "The Representation, Measurement, and Calculation of Equivalent Circuits for Waveguide Discontinuities with Application to Rectangular Slots", 1949, Chapter IV, pg. 2 et seq.

coaxial line (Microdot coaxial cable 50-3902). The outer conductor is formed by the brass housing where this will serve. In the region of the loop, the outer conductor was painted onto the teflon, and the coupling gap was carefully cut away under a microscope.

2. Measurement Technique for Dielectric-Mounted Obstacles

a) Calibration Procedure for Undesired Discontinuities

A general technique will be described which calibrates the resonance measuring setup so as to remove certain effects due to some discontinuities which may be present in the measuring cavity, in addition to the discontinuity which is to be measured. We have already carefully distinguished between discontinuities which couple many propagating modes, and those which do not couple a particular propagating mode (in particular the H_{01}^{o} mode) to any of the remaining propagating modes. In the following, all discontinuities are restricted to be of the latter type with respect to the propagating mode of interest in the measurement. Specifically then, the calibration procedure subtracts out the effects produced by the undesired discontinuities in the particular propagating mode of interest. The correction is exact if the discontinuities involved are sufficiently separated so that they do not couple appreciably via the non-propagating modes.

Several diagrams of the measuring cavity are shown in Fig. MRI-15585. The discontinuity to be measured is shown as a centered metal disk while the undesired discontinuity is shown as a dielectric slab, completely filling the guide cross section, on which the disc is mounted (Fig. MRI-15585(c)). The calibration procedure follows from Fig. MRI-15585 via a simple (rigorous) physical argument.

The first diagram, Fig. MRI-15585(a), shows a typical point in an ideal D vs S measurement where only the desired discontinuity is present in the measuring cavity. It should be remarked that although the desired discontinuity has been shown inserted at the centerline for convenience in drawing, no part of the following argument depends on this circumstance. In this first diagram, as well as in all the succeeding ones, the plungers are assumed to be positioned so that the measuring cavity is resonant in the desired (H_{01}^{o}) mode. The (ideal) data which characterizes this point of the measurement is just these plunger positions denoted D and S.

The calibration measurement D' vs S' is shown in Fig. MRI-15585(b); only the undesired discontinuities are present in the measuring cavity. First, note that the resonant condition of the cavity would not be altered if the dielectric were moved an integral number of half guide wavelengths (Figure MRI-15585(b')) because the impedance transformations performed by a length of transmission line are periodic with period $\lambda_g/2$. Second, under the assumption of no dissipation, virtual short circuits appear. In the absence of an intervening discontinuity, these are located an integral number of half guide wavelengths

from a short-circuiting plunger. Therefore, in terms of distance modulo $\lambda_g/2$ measured positive to the right of the centerline ("S distance"), the location of the virtual short circuit indicated in Fig. MRI-15585(b') is precisely S'. In terms of distance measured positive to the left of the centerline ("D distance") the same virtual short circuit is located at -S'.

The measurement of the desired discontinuity plus dielectric support, as these might be arranged in practice, is shown in Fig. MRI-15585(c). As distinct from the case of calibration just described, the measuring cavity Fig. MRI-15585(c) and the measuring cavity Fig. MRI-15585(c'), in which the dielectric support has (theoretically) been moved a number of half wavelengths to the left, are no longer exactly equivalent with respect to resonant condition. A discrepancy will arise because the two discontinuities (metal disk & dielectric) will interact via the non-propagating modes, i.e., the shunt susceptance of the disk by itself is different from the susceptance of the disk on the dielectric interface. If the dielectric constant is close to unity (as for polyfoam) the discrepancy is small and can be neglected.*

The convenient rule for subtracting out the effect of the dielectric on the propagating mode may now be inferred directly by comparing Figs. MRI-15585(a), MRI-15585(b'), and MRI-15585(c'). For a particular setting D" of the plunger in Fig. MRI-15585(c'), the location of the virtual short circuit may be read from the calibration curve D' vs S' at the point D' = D" in Fig. MRI-15585(b). This virtual short circuit position is -S' and is equivalent to the position D of the plunger in the ideal measurement (Fig. MRI-15585(a)). The position of the remaining plunger in the ideal measurement S is evidently just S".

Rule: The measurement of the desired D vs S curve (Fig. MRI-15585(a)) is reduced to the following steps:

1. Calibrate (Fig. MRI-15585(b)). Measure with only the undesired discontinuity in place, D' vs S'.

2. Measure the total structure (Fig. MRI-15585(c)), D" vs S".

3. Infer the value of D from D" and the calibration curve: D is equal to minus the value of S' corresponding to (D' equal to D") on the curve.

4. Infer the value of S from S": S is equal to S".

In symbols

$$\begin{aligned} D &= -S' \quad , \qquad D'' = D' \Longrightarrow S' \\ S &= S'' \end{aligned}$$

where $\Longrightarrow$ means via calibration curve D' vs S'.

---

* The magnitude of this interaction as it affects the H_{01}^0 susceptance has been estimated theoretically (see Sec. C(g)).

The calibration procedure outlined above is easily generalized to the case where undesired discontinuities occur on both sides of the structure to be measured provided that, as in the above illustration, it is possible to remove any of the discontinuities from the measuring cavity as desired. Then it is merely necessary to perform an additional calibration measurement, call it D''' vs S''', with only the additional undesired discontinuity present in the measuring cavity. The correction rule may then be stated:

Rule: $D = -S'$, $D'' = D' \Longrightarrow S'$

$S = -D'''$, $S'' = S''' \Longrightarrow D'''$

The statement of the rule is now symmetrical in D and S as one would expect from the symmetric definitions of the parameters D & S.

b) Independent Check of the Calibration Procedure for Dielectric-Mounted Obstacles

Several of the discontinuities which have been investigated theoretically and for which approximate H^o_{o1} equivalent circuit parameters have been computed, consist of thin metallic obstacles suspended in a transverse section of the uniform waveguide. This condition may be achieved in practice by embedding the obstacle in guide filled with a solid dielectric, the dielectric extending on either side of the obstacle for a distance sufficient to allow the amplitudes non-propagating modes decay to negligible values. However, it is generally more convenient to mount the obstacles on a relatively thin sheet of material the dielectric constant of which is very nearly that of free space, e.g., polyfoam. This latter alternative has been adopted in the measurements which have been made of

1. The centered circular disk
2. The pseudo-symmetric arrangement of disks

A theoretical estimate of the effect of the polyfoam mount may be obtained for the circular disk from the formulae developed in Q4 and graphed as MRI-15177. These results are graphed in a more significant form in Fig. MRI-15581 included in this report. The dielectric constant of the polyfoam may be taken as 1.06.

The effect of the dielectric support on the H^o_{o1} mode can be subtracted out via a general calibration procedure described in detail in the preceding section. As a check on this subtraction procedure the susceptance of a centered circular aperture, which can be measured without any dielectric support, was measured under the following conditions: (1) The aperture discontinuity was placed in the guide by itself. (2) The aperture was placed as in (1) and a 1" thick polyfoam slab placed adjacent to it. (3) The polyfoam slab was measured separately. (4) The aperture and support were placed as in (2) but (3) was utilized to subtract the effect of the support. (5) The aperture was placed as in (1) and a polyfoam slab placed $\lambda_{g(o1)}/2$ removed from the aperture plane. The results of these measurements are recorded in Table I. The aperture employed in this test had a value of $(r_o/a) = .90$ (r_o = aperture radius, a = guide radius),

and the measurements were carried out at a frequency corresponding to $a/\lambda = 0.75$. (Note: It is impermissible to add (or subtract) the equivalent susceptances of the aperture and support since they do not occur at the same reference plane.)

TABLE I

	Identification	Insertion VSWR ($-\gamma$)	Magnitude of Normalized Equivalent Susceptance $-(B_a/Y_o \lambda_g)$	Spread of D+S vs S Curve (in.) ($2\Delta_m$)
1	Aperture alone	1.196	.0782	.187
2	Aperture + support	1.167	.0677	.163
3	Support alone	1.082	(.0345)	.0828
4	(Aperture + support) - (support)	1.194	.0777	.186
5	(Aperture + $\lambda_g/2$ + support)-(support)	1.200	.0799	.191

The direct check on the calibration procedure follows from comparison of (1) and (5) which should be identical but differ by .0017 (second column). This difference may be due in part to inability to position the polyfoam disk accurately within the cavity. The entries (1) and (4) should differ by the higher mode interaction between the aperture and the dielectric. The dielectric is positioned at the end of the cavity flange for the measurement (4) and is in the same position in the calibration measurement (3). For this reason the result (4) is probably more accurate than (5). It is seen that the difference between (1) and (4) is small and can be neglected. The difference between (4) and (1) may be compared with the theoretical calculation for an aperture next to a dielectric interface contained in Q4 and graphed as MRI-15178 (see also Figure MRI-15581). If the dielectric constant of polyfoam is taken as 1.06,

$$\Delta(B_a)/(Y_o\lambda_g) = +.0006 \text{ as compared with } (4)-(1) = (-.0777)-(-.0782) = +.0005$$

from Table I. No detailed comments on the precision of these latter figures will be made here. However, it is noted that the difference between measurements (4) and (5) is extremely small and in the direction expected from the approximate theory.

IV. Overall Conclusions

The conclusions and results reached from investigations under this contract are summarized in the Abstract.

V. Recommendations

A more comprehensive future program in the study of multimode propagation, transcending the aims described in this report, suggests itself. There exist, broadly speaking, two major categories: a) the description of single discontinuities in a multimode structure, and b) the effect of several known discontinuities on the propagation of the electromagnetic fields. The former is an electromagnetic field problem, while the latter poses a multi-transmission line network problem. Whereas for single-mode propagation the field problem is usually the more formidable, for multimode propagation the network problem is likewise exceedingly complicated. The study of multimode phenomena (both field and network problems) may be approached either by extension of known single-mode theory, or by modification of optical (infinite number of modes) descriptions. On this contract, emphasis has been placed so far exclusively on the former technique which is most appropriate when the number of propagating modes is small; the optical approach is, however, worthy of serious consideration and should be further exploited.

A very interesting class of network problems arises when a multimode waveguide is periodically loaded. The effect of two small discontinuities has already been described in this report. If a large number of identical discontinuities is employed a periodic structure results whose effects on multimode propagation as regards frequency pass and stop-bands, etc., should be of considerable interest. The methods employed in the analysis of such configurations would be extensions of single-transmission-line periodic-structure techniques.

The experimental program should be extended to the measurement of discontinuities in the presence of several interacting modes, thus transcending the present measurement program which has concerned itself with TE_{01} mode measurements only. The cavity setup which has been constructed for the TE_{01} mode measurements can readily be adapted to measure interaction at a symmetric discontinuity between TE_{11} and TM_{11} modes by a resonance method. This would be the first step toward multimode measurements by a resonant cavity technique and is of interest in the analysis of propagation of the lowest mode in a circular guide which can also propagate the TM_{11} mode. The possibilities of other measurements by this technique remain to be explored.

VI. Personnel

The following professional personnel have been associated with this contract during the final quarter:

L. B. Felsen	199 hours
J. Fox	17 hours
J. W. E. Griemsmann	18 hours
H. Hanft	7 hours
W. K. Kahn	422 hours
N. Marcuvitz	35 hours
A. A. Oliner	35 hours

APPENDIX I

Components List

Source Assembly

1.	Power Supply	-	Polytechnic Research & Development Corporation (PRD) Type 801A Power Supply.
2.	Oscillator	-	PRD Type 708 Broadband Microwave Oscillator. Frequency range 2.0 - 4.8 kmc.
3.	Attenuators	-	PRD Type 130 or 1100. Frequency range to 4 kmc. Insertion VSWR less than 1.4.
4.	Filter	-	Microlab FL-4000 Coaxial Low Pass Filter. Cutoff frequency 4.0 kmc, second resonance at 20 kmc.
5.	Crystal Detector	-	PRD Type 613-M. 1N23 crystal. Frequency range 1 to 10 kmc.
6.	Oscilloscope	-	Du Mont Type 304 Cathode Ray Oscilloscope.

Frequency Monitoring Assembly

7.	Attenuators	-	See 3 above.
8.	Crystal Detector	-	See 5 above.
9.	Wave Meter	-	Micro Instrument Company. Coaxial Transmission Wave Meter. Frequency Range 1.5 to 6 kmc or 6-20 cm (free space wavelength).
10.	Amplifier	-	PRD Type 277 Standing Wave Amplifier.

Cavity Assembly

11.	Measuring Cavity	-	Fabricated at MRI. Described in drawings MRI-15499 & MRI-15500.
12.	Attenuators	-	See 3 above.
13.	Amplifier	-	See 10 above.

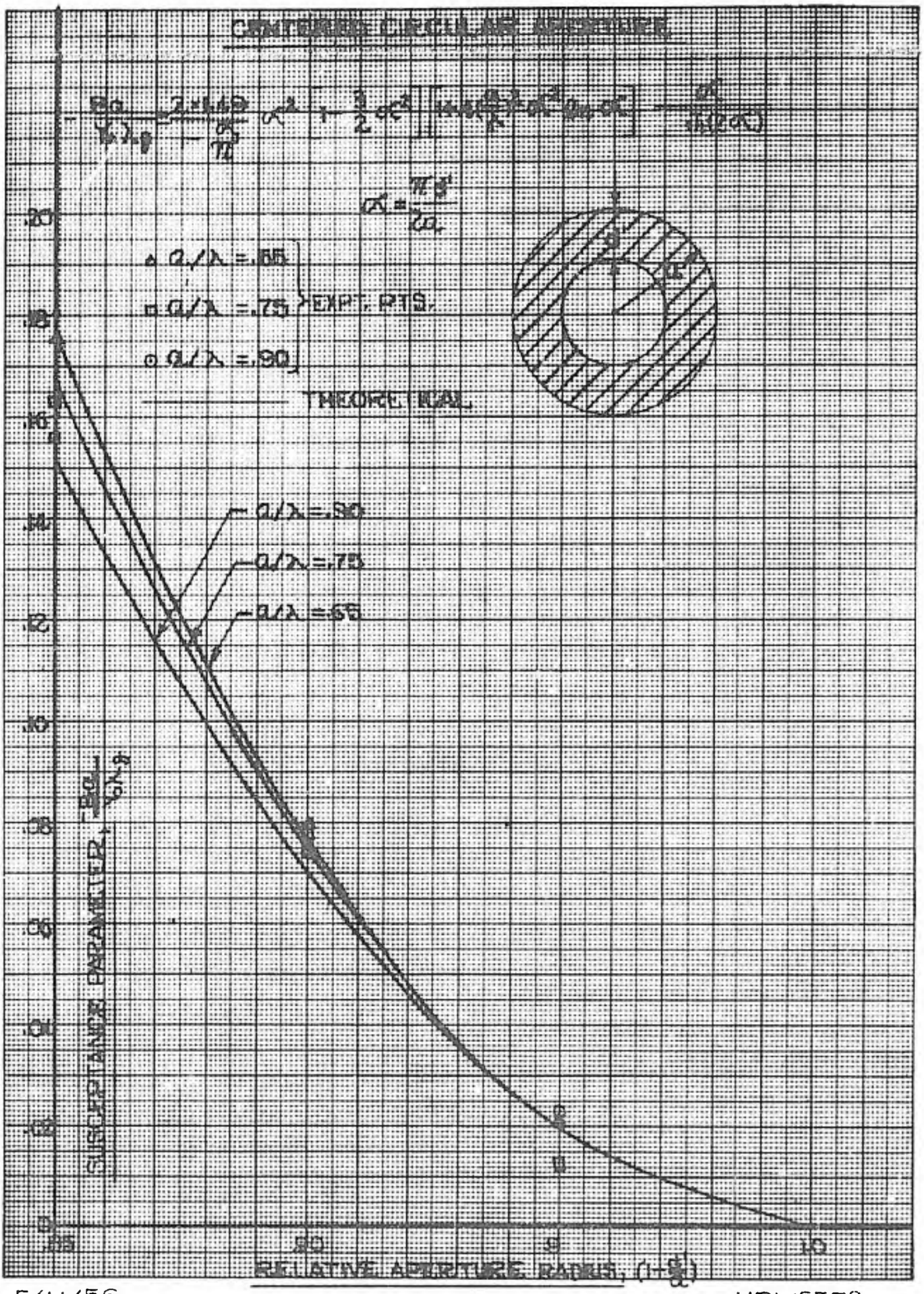

5/11/56

MRI 15572

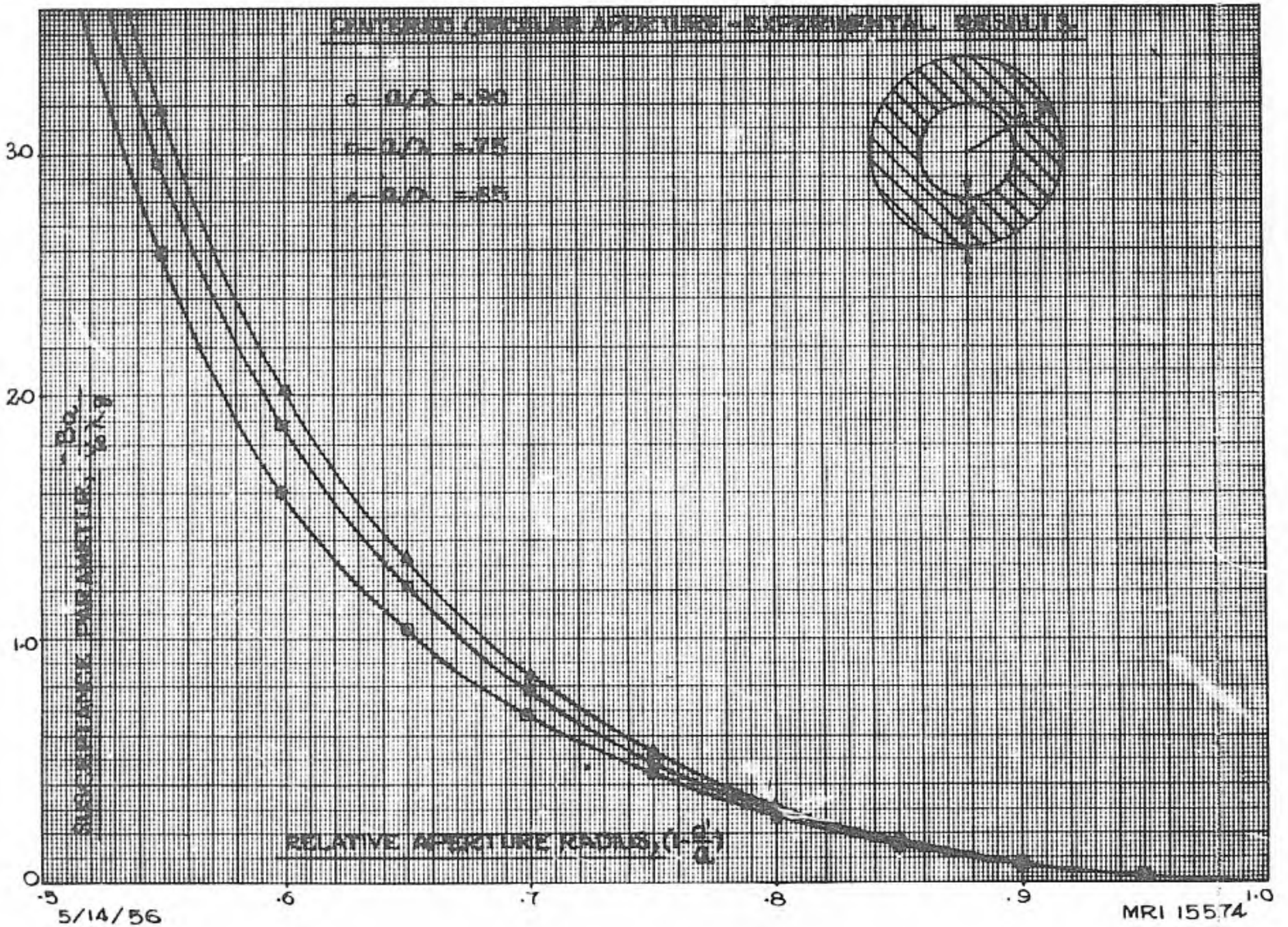
CAUCHOIS CIRCULAR APERTURE - EXPERIMENTAL RESULTS
a - a/A = .90
b - a/A = .75
c - a/A = .55
SUPERTANGK PARAMETER, $\frac{B\alpha}{\sqrt{\alpha^2 k^2}}$
RELATIVE APERTURE RADIUS $(1-\frac{a'}{a})$
3.0
2.0
1.0
0
.5
.6
.7
.8
.9
1.0
5/14/56
MRI 1557A

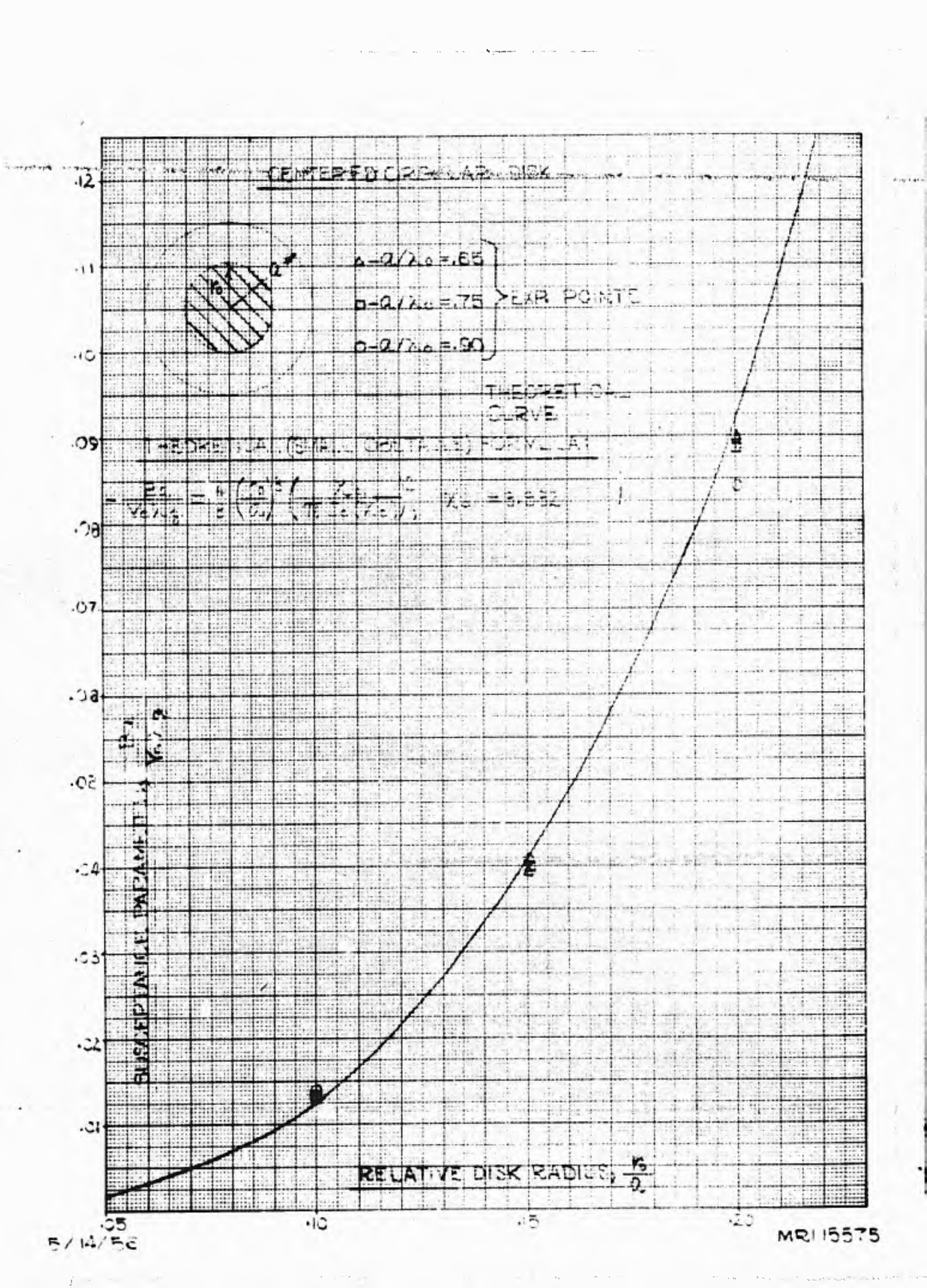
CENTERFED CIRCULAR DISK
a=2/λ0=.65
a=2/λ0=.75
a=2/λ0=.50
EXACT POINTS
THEORETICAL CURVE
THEORETICAL (TRIAL CABLE) FORMULA
SUSCEPTANCE PARAMETER
RELATIVE DISK RADIUS, r0/λ0
.12
.11
.10
.09
.08
.07
.06
.04
.02
.01
.05
.10
.15
.20
5/14/58
MRI 15575

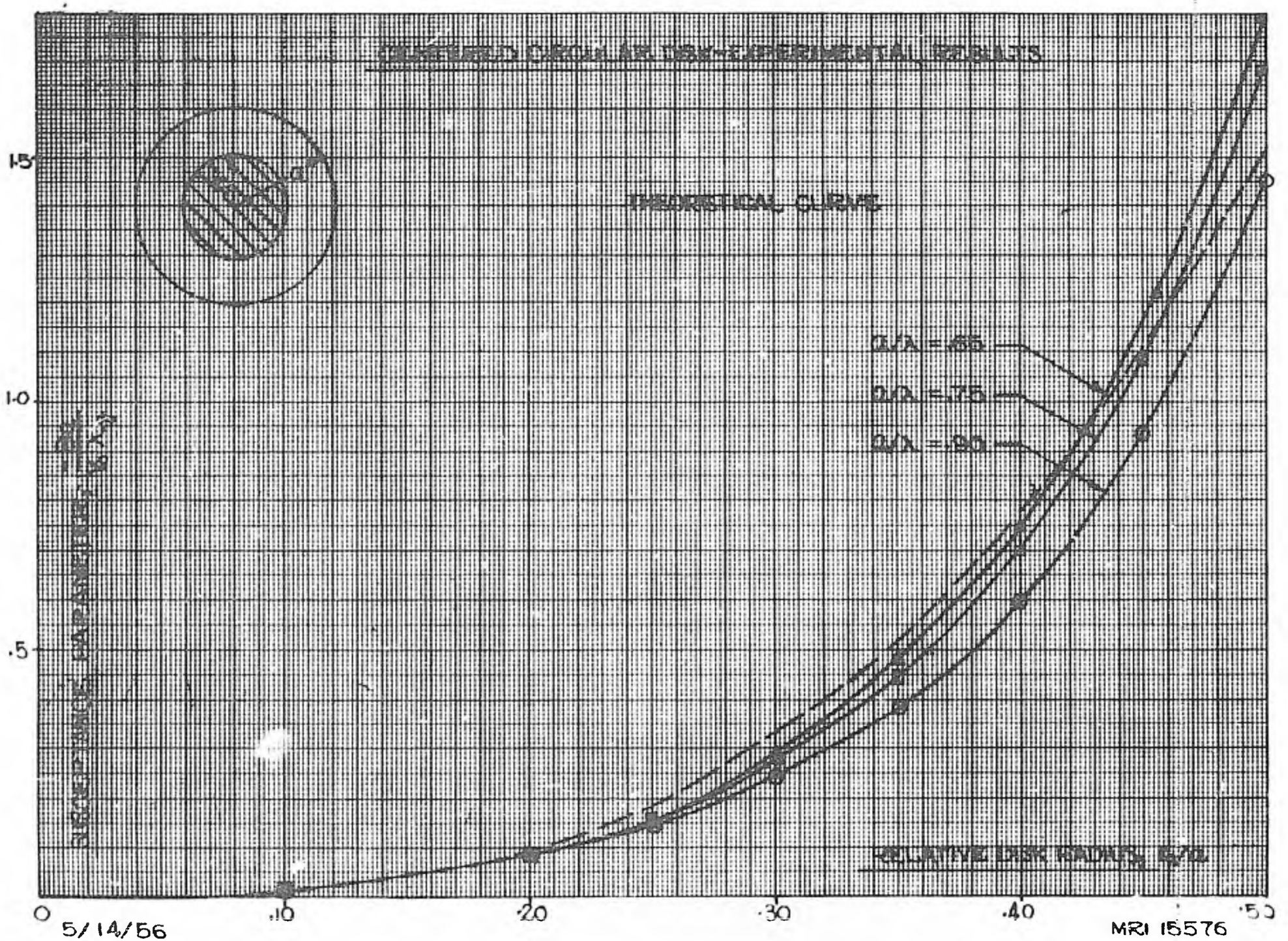
SHIELDED CIRCULAR DISK-EXPERIMENTAL RESULTS
THEORETICAL CURVE
D/λ = .65
D/λ = .75
D/λ = .90
SCATTERING PARAMETER
RELATIVE DISK RADIUS, a/λ
1.5
1.0
.5
0
.10
.20
.30
.40
.50
5/14/56
MRI 15576

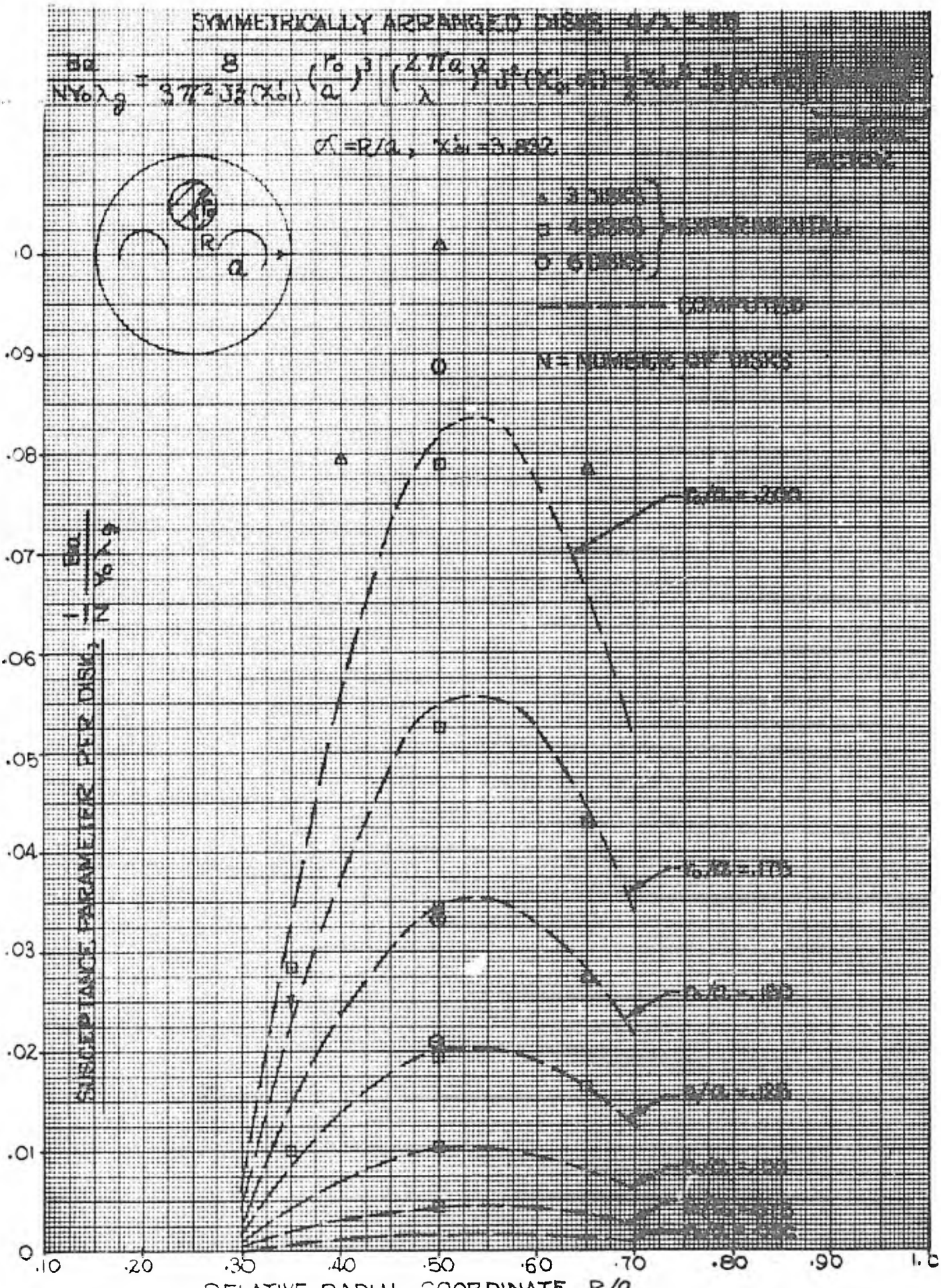

5/14/56

MRI 15577

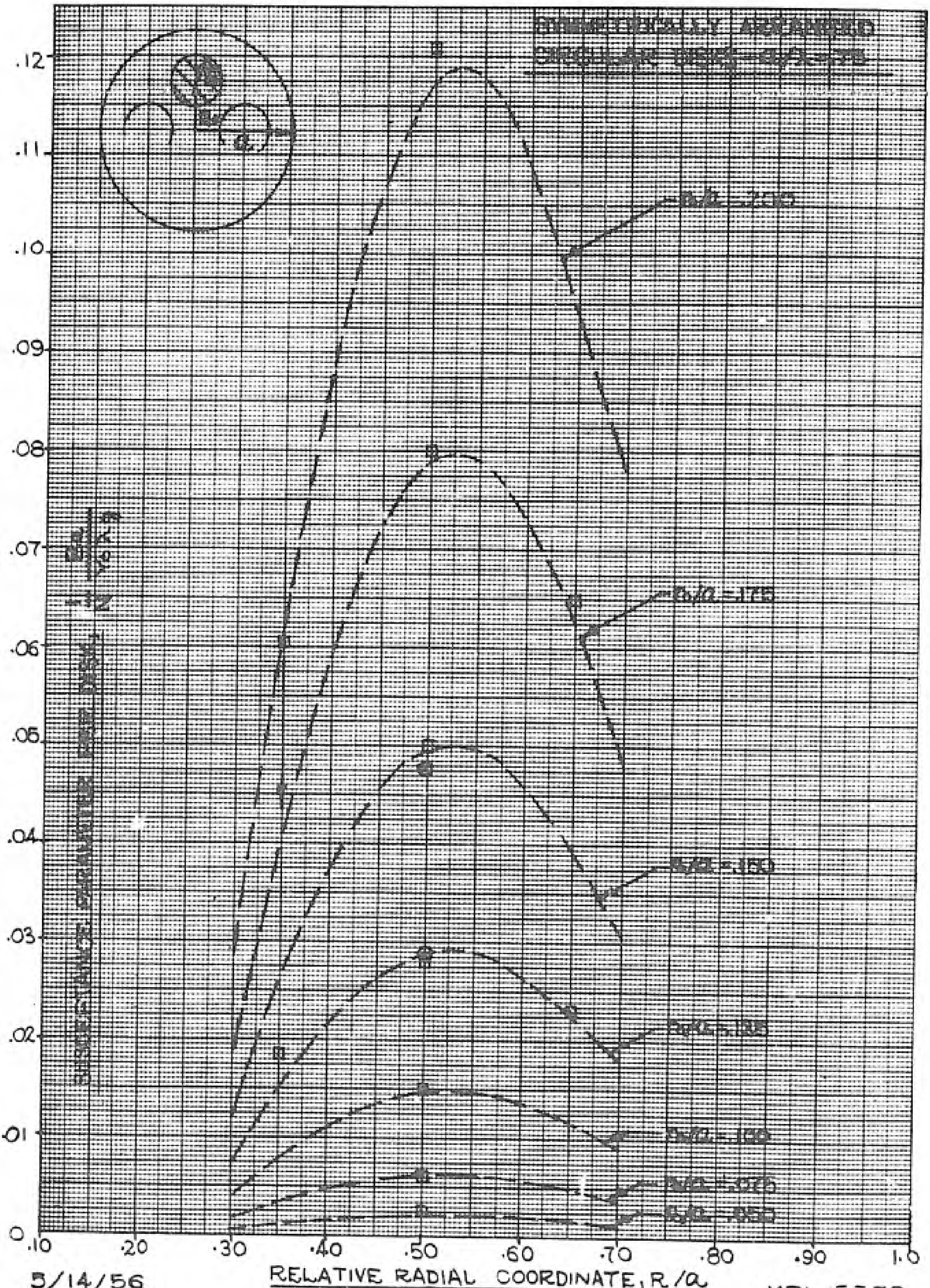

5/14/56

MRI 5578

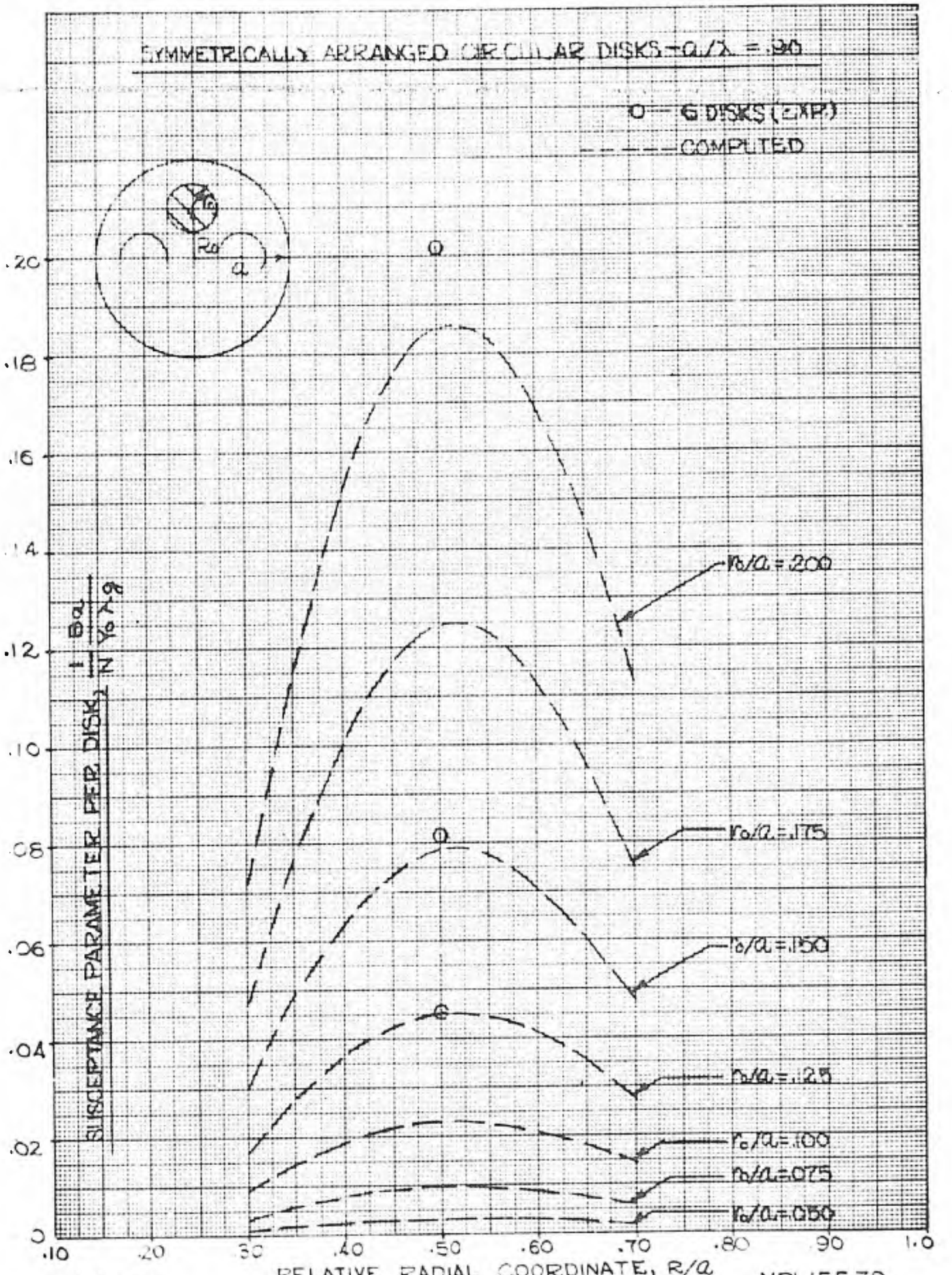

5/14/56

MRI 1557 9

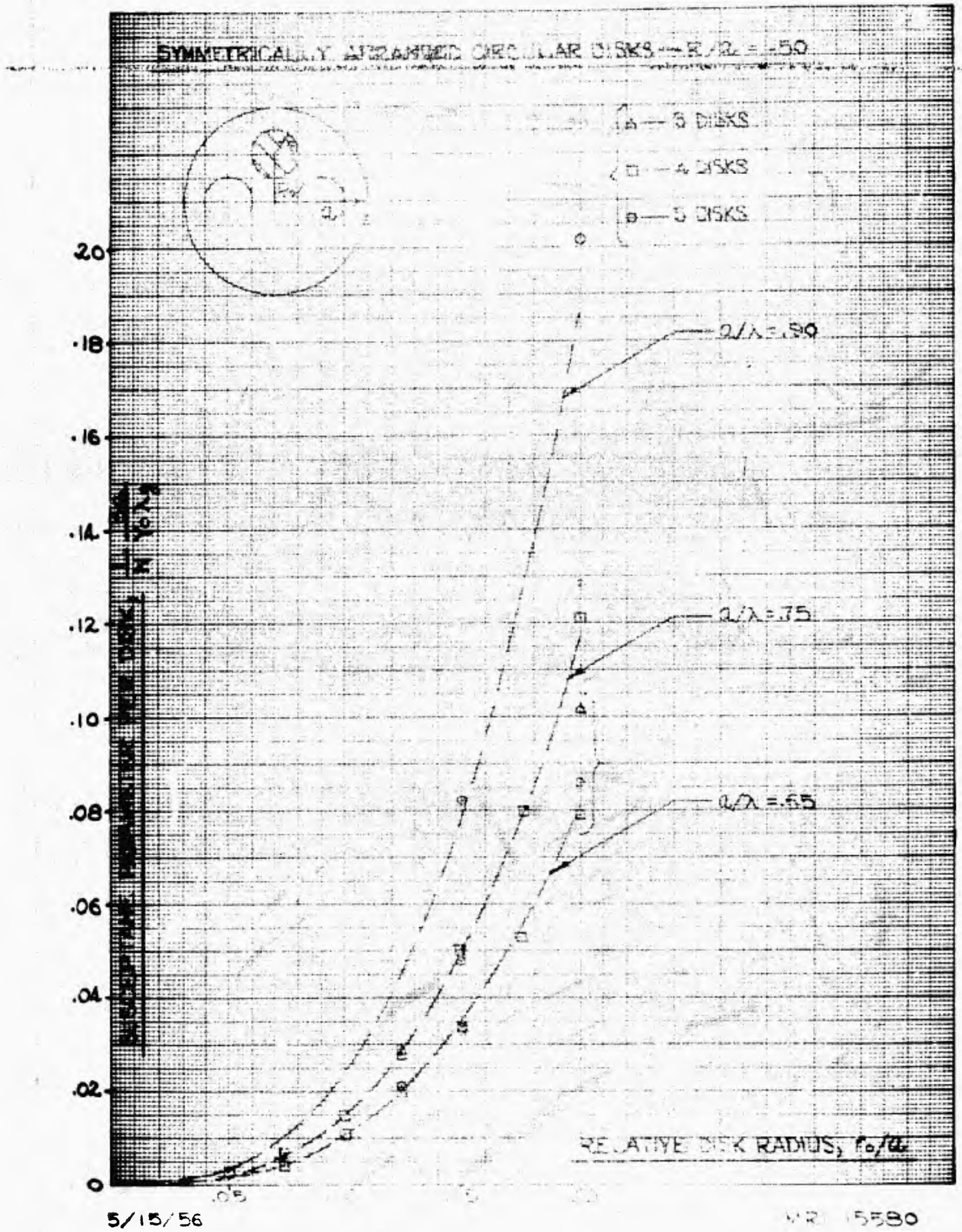

5/15/56

MR 5580

CORRECTION TO SUSCEPTANCE OF A GROUNDED CIRCULAR DISK FOR PRESENCE OF DIELECTRIC INTERFACE:

$$\Delta\left(\frac{B a_1}{Y_0 \lambda_g}\right)_{air} = \frac{B a_1}{Y_0 \lambda_g} (\epsilon - 1)$$

(FOR a_1 SEE QUARTERLY REPORT #4, PART I 3(d))

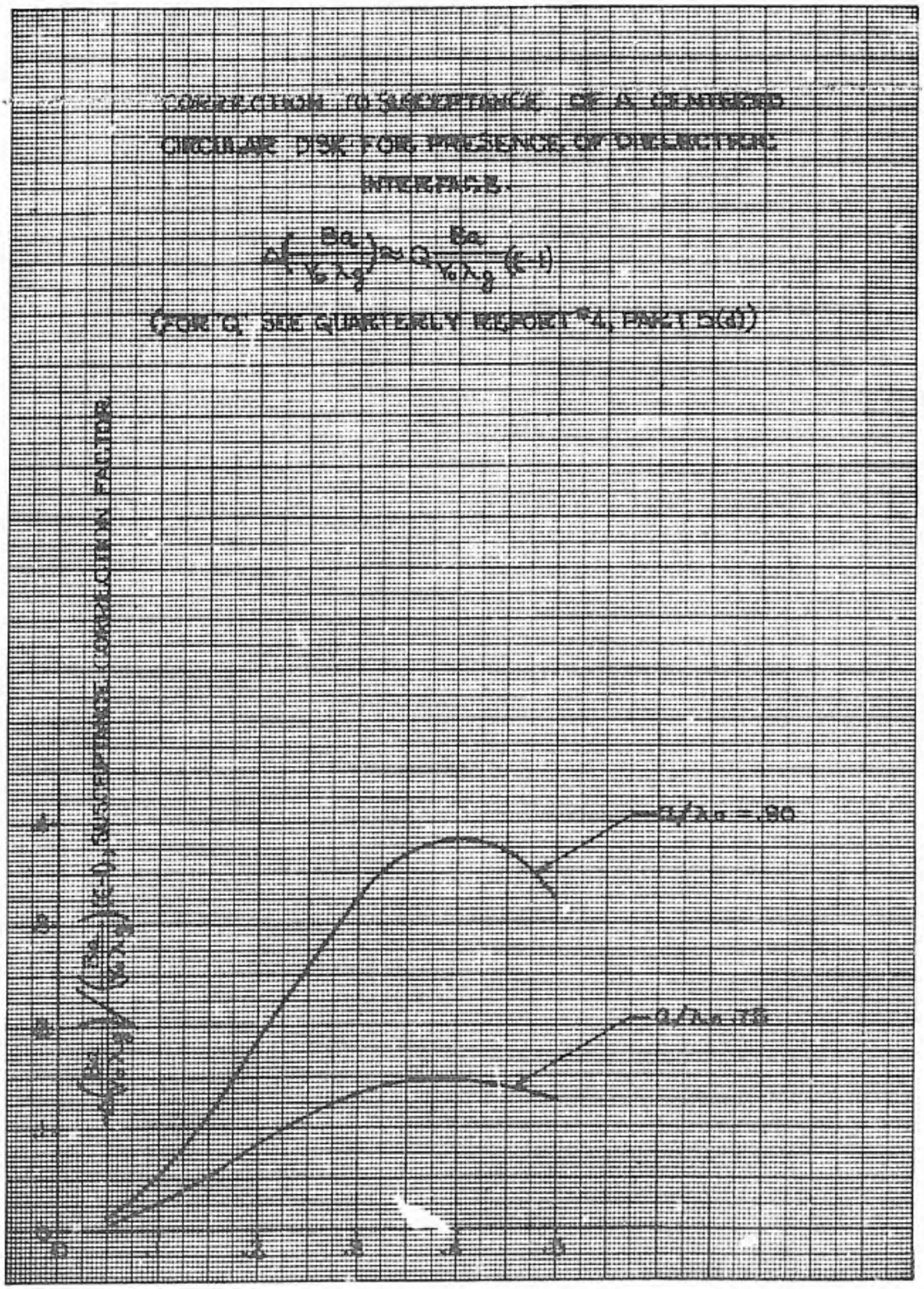

5/14/56

MRI 1558I

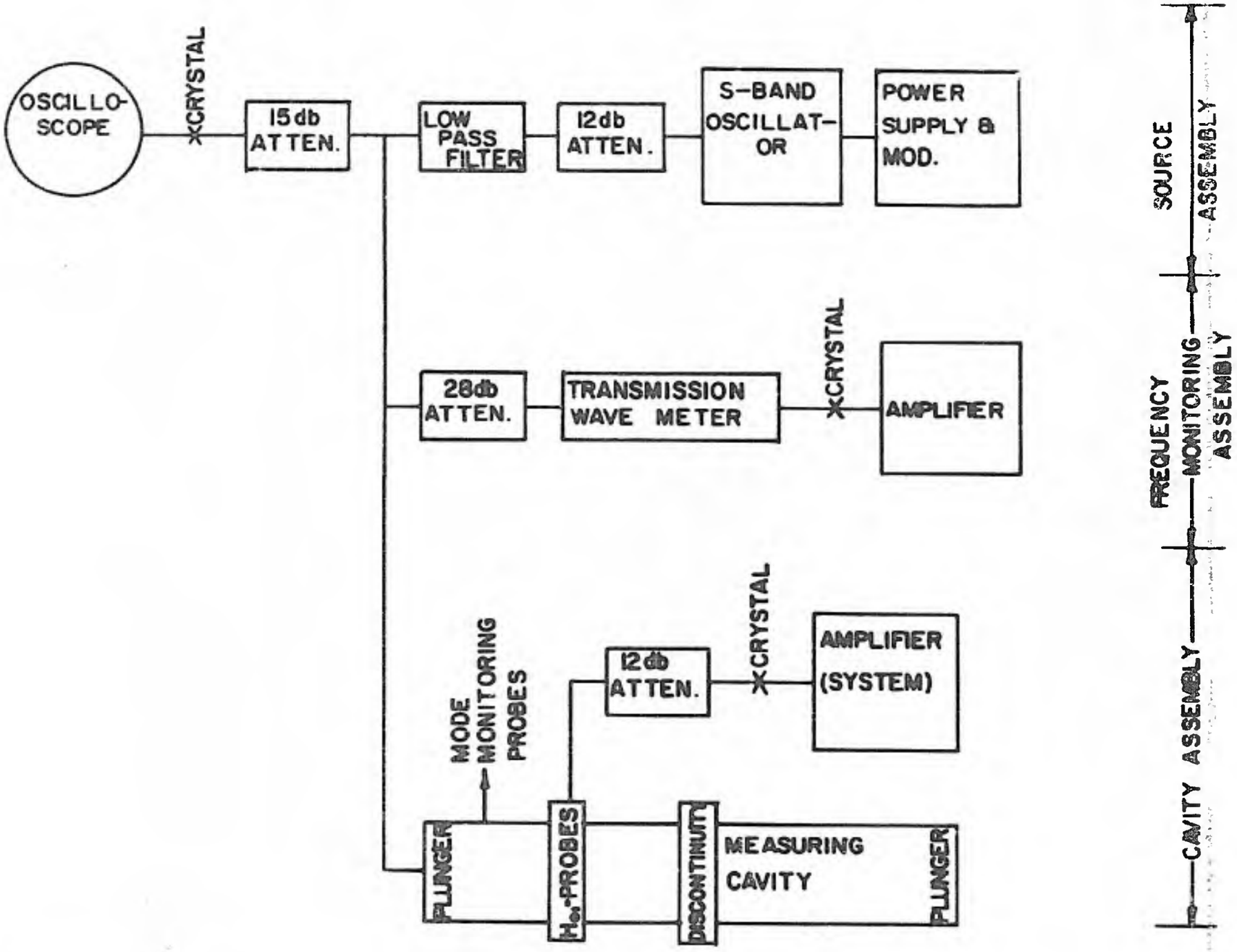

RESONANCE MEASURING SET-UP, BLOCK DIAGRAM

MRI 15582

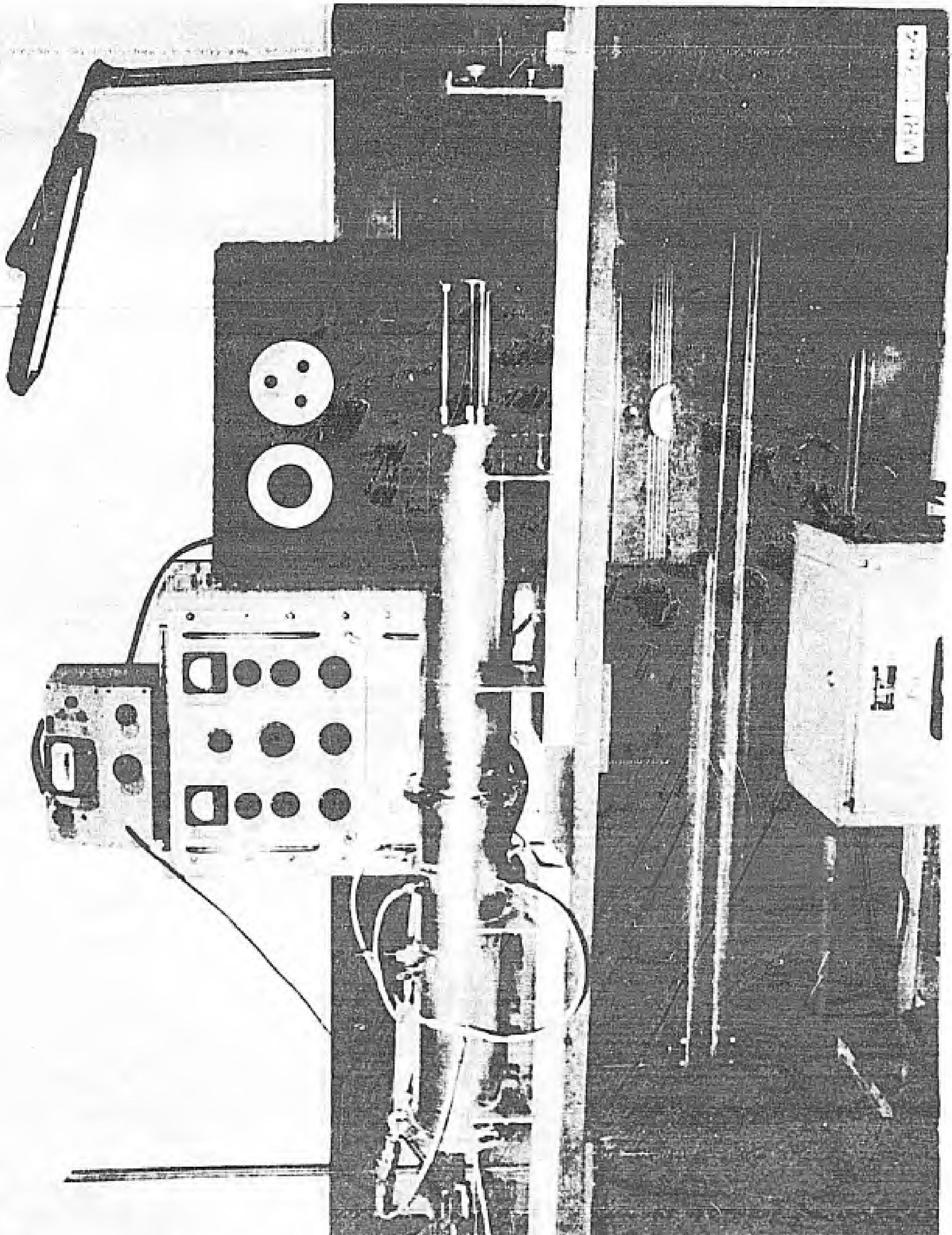

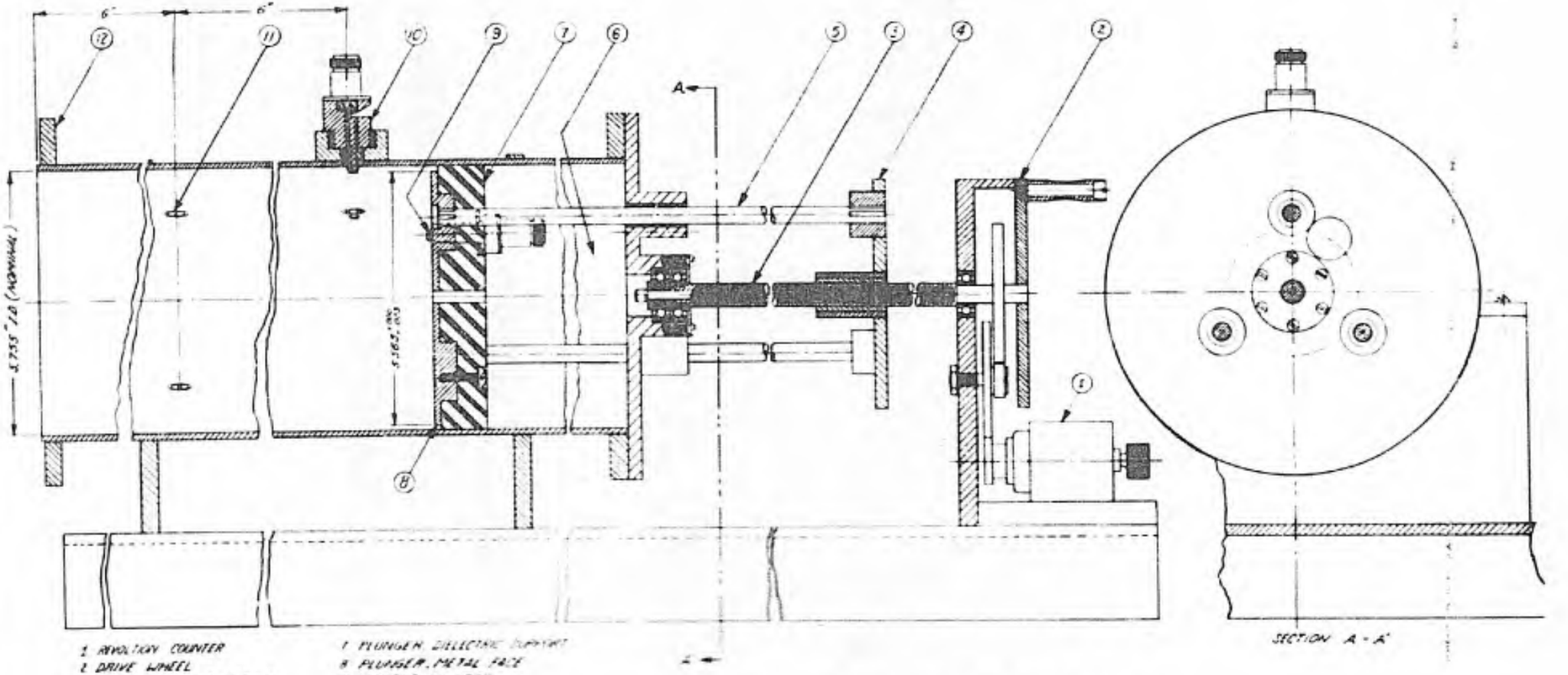

1. REVOLUTION COUNTER
2. DRIVE WHEEL
3. PRECISION DRIVE SCREW
4. TIE PLATE
5. DRILL RODS
6. DISSIPATIVE MATERIAL

7. PLUNGER, DIELECTRIC SUPPORT
8. PLUNGER, METAL FACE
9. EXCITATION LOOP
10. MONITOR LOOP
11. DETECTOR LOOP
12. FLANGE

LONGITUDINAL SECTION OF MEASURING CAVITY

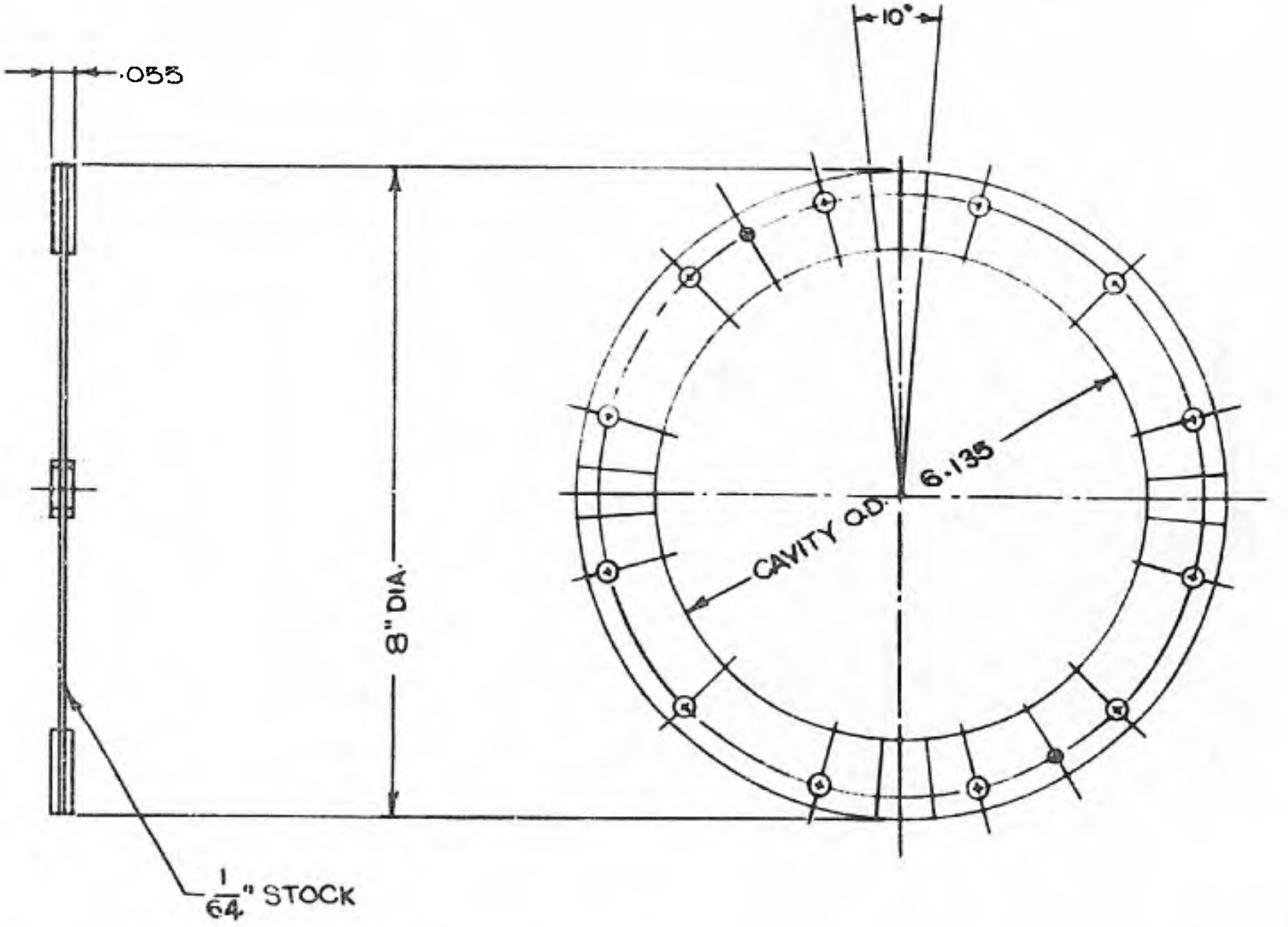

JIG FOR THIN APERTURE DISCONTINUITIES

5/11/56

MRI 15583

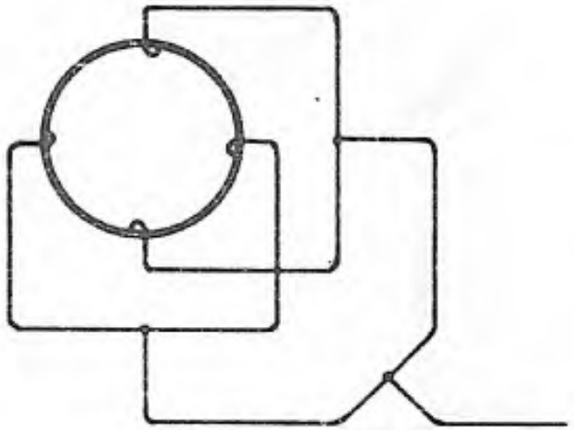

SYMMETRICAL INTERCONNECTION OF DETECTOR LOOP PROBES

MRI-5584-A

PROBE

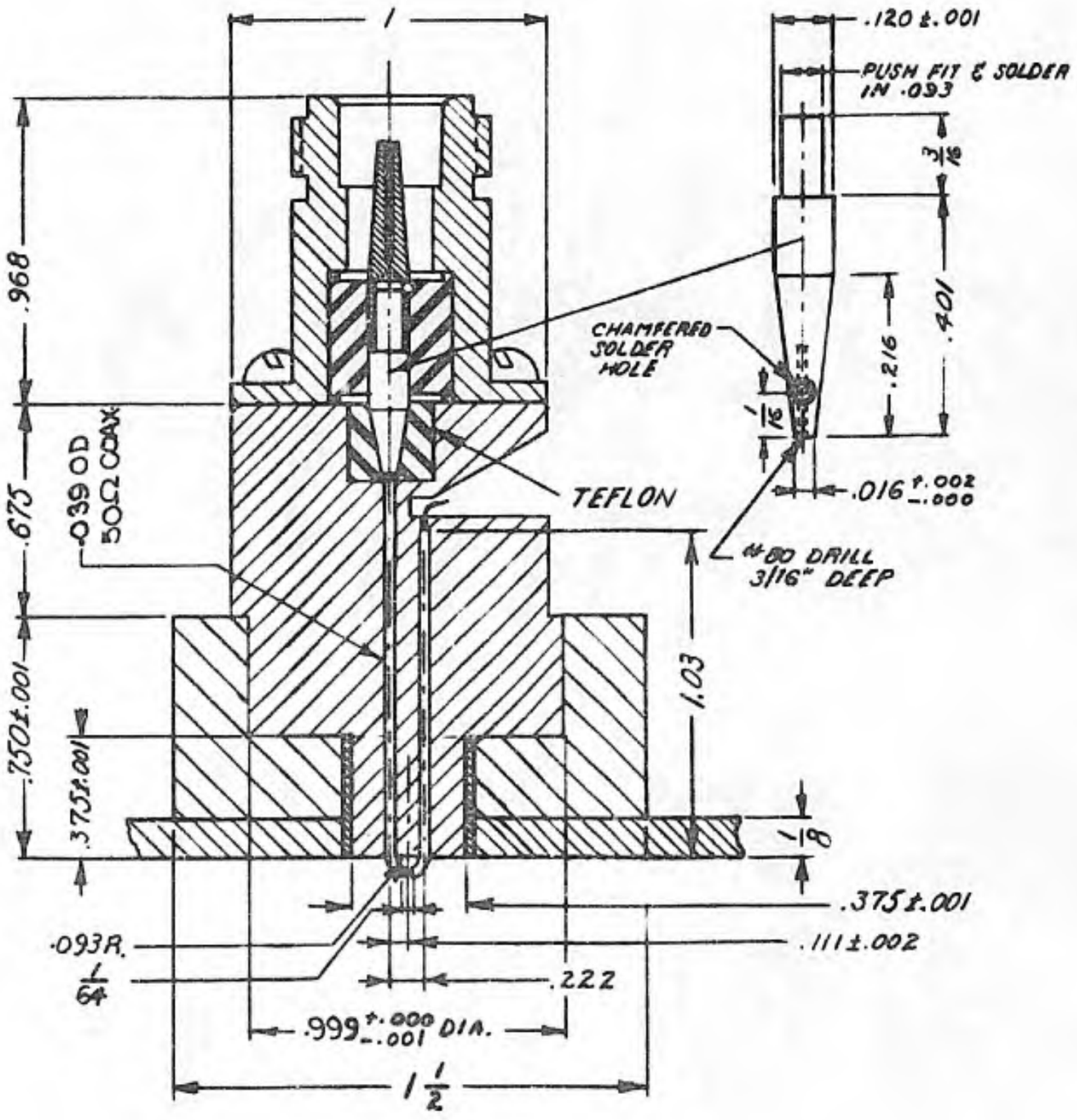
1
.120 ±.001
PUSH FIT & SOLDER IN .093
3/16
.968
.401
.216
CHAMFERED SOLDER HOLE
1/16
.016 +.002 -.000
.039 OD 50Ω COAX
TEFLON
#80 DRILL 3/16" DEEP
.675
.750±.001
1.03
.375±.001
1/8
.375±.001
.093R.
1/64
.111±.002
.222
.999 +.000 -.001 DIA.
1 1/2

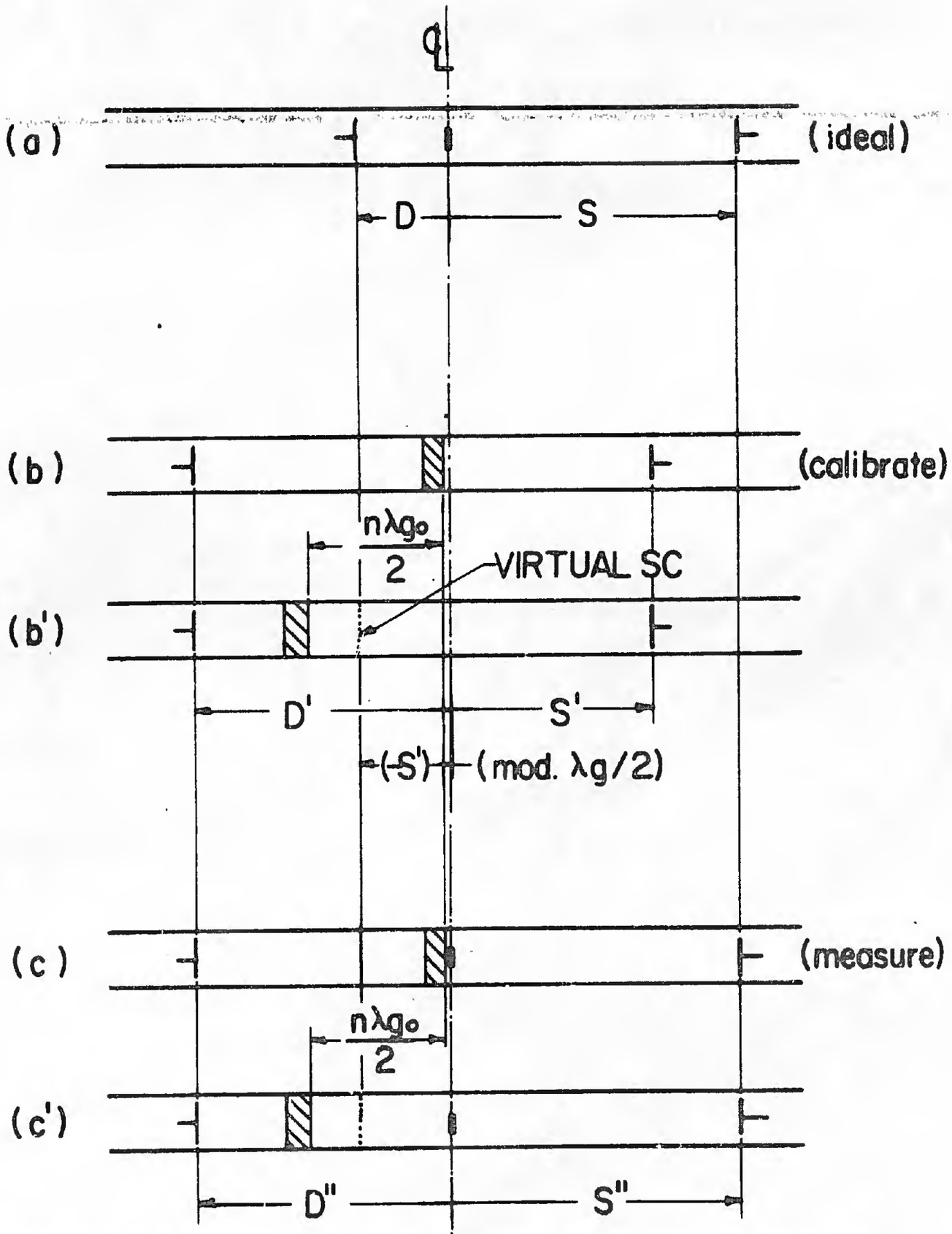

MEASURING CAVITY DIAGRAMS FOR CALIBRATION PROCEDURE

MRI 15585